ISSN: 2738-9928 (Online)
2738-9812 (Print)

NEPAL JOURNAL OF MATHEMATICAL SCIENCES (NJMS)

Published by

SCHOOL OF MATHEMATICAL SCIENCES

Tribhuvan University, Kirtipur
Kathmandu, Nepal

Volume 6, Number 1 **February 2025**

NEPAL JOURNAL OF MATHEMATICAL SCIENCES (NJMS)

ISSN: 2738-9928 (Online), 2738-9812 (Print)

Volume-6, Number -1 (February 2025)

NEPAL JOURNAL OF MATHEMATICAL)SCIENCES (NJMS
Volume-6, Number-1 (February, 2025)

The Nepal Journal of Mathematical Sciences (NJMS) is now available on NepJOL at https://www.nepjol.info/index.php/njmathsci/index

MAILING ADDRESS

Nepal Journal of Mathematical Sciences
School of Mathematical Sciences
Tribhuvan University, Kirtipur
Kathmandu, Nepal
Website: www.sms.tu.edu.np
Email: *njmseditor@gmail.com*

Editorial

We are pleased to announce the release of the first issue of Volume 6 of the *Nepal Journal of Mathematical Sciences (NJMS)* for the year 2025. This issue features six research articles that cover a wide range of topics in mathematics and mathematical sciences.

We would like to express our sincere gratitude to all the authors for their valuable contributions to this issue. Our heartfelt thanks also go to the reviewers and editors for their dedicated support and expert guidance, which have been crucial in bringing this publication to life.

We extend an invitation to professors, research scholars, and scientists to submit their original research work for consideration in future issues of NJMS. Your contributions are vital to advancing the field of mathematical sciences and enriching the scholarly community.

Thank you for your continued support.

Editor-in-Chief
April 8, 2025

CONTENTS

Nepal Journal of Mathematical Sciences (NJMS)
ISSN: **2738-9928** (*online*), **2738-9812** (*print*)
Vol. 6, No. 1, 2025 (February): **1-6**
DOI: 10.3126/njmathsci.v6i1.77368

Research Article
Received Date: August 15, 2024
Accepted Date: January 10, 2025
Published Date: April 8, 2025

On ϑ – Curvature Tensor of Finslerian Hypersurfaces Given by Generalised Kropina Type Metric

Poonam Miyan[1*], Hemlata Pande[2] & Dhirendra Thakur[3]

[1] *Department of Mathematics, L.B.S.G.P.G. College, Halduchaur, Nainital, India*

[2] *Department of Mathematics, Government P.G.College Bageshwar, India*

[3] *Department of Mathematics, Kailali Multiple Campus, Far Western University, Nepal*

Corresponding Author: [*]poocares4u@gmail.com

Abstract: *The purpose of the present paper is to find angular metric tensor ,carton torsion tensor, v-curvature tensor in a generalized Kropina space and the relation between v -curvatures with respect to Cartan connection $C\Gamma$ of a Finsler space $F^n = (M^n, L)$ and a Finsler space $F^{*n} = (M^n, L^*)$ whose metric L^* is derived from the metric L of F^n by $L^* (x, y) = \mu^{1/2} (x, y) \beta^{1/2} (x, y)$, where $\mu^{1/2} (x, y) = (L^{1/2} + \beta^{1/2}) (x, y)$ and $\beta = b_i(x) y^i$. The Finsler space F^{*n} is called a generalized Kropina space under certain conditions.*

Keywords: *Finsler metric, Kropina space, Cartan connection, h- vectors ϑ -curvature tensor.*

Mathematics subject classification: 2000: 53B 20, 53B 28, 53B 40, 53B 18.

1. Introduction

The study of Finsler spaces, with special metrics, has attracted considerable attention over the years. Among these, the Kropina metric, introduced by V.K. Kropina, has been a focal point due to its unique properties and applications. The Kropina metric is a special case of the (α, β)-metric, where the metric function is given by

$$L(x, y) = \frac{\alpha^2}{\beta},$$

with α being a Riemannian metric and β a 1-form.

This metric has been extensively studied in the context of Finslerian hypersurfaces, where the interplay between the intrinsic and induced geometries provides deep insights into the structure of the space.

A significant milestone in the development of Finslerian hypersurfaces was the introduction of the Kropina metric by Kropina himself. This class of Finsler metrics, given by

$$L(x, y) = \alpha^m \beta^n \text{ (where } m \neq 0, -1)$$

was extensively studied by Shibata [8], who investigated its geometrical properties and provided foundational results on its structure. Later, Shibata et al. [9] extended this work by introducing the transformation of Finsler metrics using

$$L^{*}(x,y) = f(L,\beta), \tag{1}$$

where f is a positively homogeneous function of degree one in L. This transformation played a crucial role in understanding the induced and intrinsic theories of hypersurfaces in Kropina spaces.

Hashiguchi et al. [1] studied the properties of Landsberg spaces with (α,β) metrics, providing insights into two-dimensional Finslerian structures. Their work was further expanded by Kitayama [2], who explored metric transformations and their impact on hypersurfaces in Finsler spaces. Additionally, Matsumoto [3] developed the induced and intrinsic connections of Finslerian hypersurfaces, contributing significantly to the study of projective geometry in Finsler spaces.

Prasad [4] and Prasad & Tripathi [5] examined torsion tensors and hypersurface structures in Finsler spaces with Kropina changes, establishing important results on the interactions between different types of metric transformations. Rastogi [6] extended these ideas by analyzing the properties of (α,β) metrics, further refining our understanding of Finslerian geometry.

Recent studies have continued to build on these foundational works. Shanker et al. [7] investigated curvature properties in homogeneous Finsler spaces, revealing new relationships between curvature tensors and metric deformations. Singh et al. [10] and Singh & Srivastava [11] explored h-transformations and Kropina-type modifications in special Finsler spaces, shedding light on the structural modifications induced by such transformations.

Izumi introduced the concept of h-vectors b_i that are ϑ-covariantly constant with respect to the Cartan connection, leading to new insights into the interplay between conformal transformations and directional dependencies in Finsler spaces. Srivastava and Pandey [12] , [13], extended this idea by examining generalized Kropina-type metrics under β-change and their implications for Finslerian hypersurfaces. Their work provided key relations between the original and transformed hypersurfaces, establishing conditions under which these transformations preserve geometric properties.

In this paper, we consider a generalized Kropina-type metric given by:

$$L^{*}(x,y) = \mu^{1/2}(x,y)\beta^{1/2}(x,y), \tag{2}$$

where

$$\mu^{1/2}(x,y) = \left(L^{1/2} + \beta^{1/2}\right)(x,y) \text{ and } \beta = b_i y^i,$$

with the vector b_i as a function of positional coordinates x^i only. When $L(x,y)$ corresponds to a Riemannian space, $L^{*}(x,y)$ reduces to the Kropina metric function.

Izumi while studying a conformal transformation of a Finsler space, introduced the h – vector b_i which is ϑ covariantly constant with respect to Cartan connection CΓ and

$$LC_{hij}\, b^h = \rho\, h_{ij}.$$

The h – vector b_i is not only a function of positional coordinates x^i but also a function of directional arguments y^i. In fact

$$L(\partial b_i / \partial y^j) = \rho\, h_{ij}.$$

Here $b_i(x, y)$ is an h – vector in (M^n, L).

Let b_i is an h-vector in the Finsler space (M^n, L) and (M^n, L^*) be another Finsler space. The fundamental metric function $L^*(x, y)$ is defined by

$$L^{*}(x,y) = (L^{1/2} + \beta^{1/2})(x,y)\,\beta^{1/2}(x,y). \tag{3}$$

Let us call the Finsler space $F^{n*} = (M^n, L^*)$ as generalazed Kropina space. To distinguish the geometrical objects of F^{n*} from those of the Finsler space F^n, we shall put *a* * sign on the corresponding objects of F^n.

This metric plays a crucial role in analyzing the curvature properties of Finslerian hypersurfaces, particularly through the ϑ-curvature tensor, which provides insights into the geometric deformations induced by the generalized Kropina-type metric.

Building upon the existing body of research, this study aims to further examine the properties of Finslerian hypersurfaces defined by the generalized Kropina-type metric and analyze the implications of the ϑ-curvature tensor in this context.

For an *h*-vector b_i we have the following lemmas [1] :

Lemma 1. If b_i is an *h*-vector then the function ρ and $l^*_i = b_i - \rho l_i$ are independent of *y*.

Lemma 2. The magnitude of an h-vector b_i is independent of *y*.

2. Preliminaries

Let b_i is a vector field in the Finsler space (M^n, L). If b_i satisfy the conditions [4]

$$b_{i|j} = 0$$

and
$$LC^h_{ij}\, b_h = \rho\, h_{ij}, \tag{4}$$

then the vector field b_i is called an *h*-vector. Here $|_j$ denotes the covariant differentiation with respect to Cartan's connection CΓ, C_{hij} is the Cartan's C-tensor, h_{ij} is the angular metric tensor, and ρ is a function described by

$$\rho = (n-1)^{-1} L\, C^i\, b_i, \tag{5}$$

We have $\frac{\partial\beta}{\partial y^i} = b_i$ by using the indicatory property.

Differentiating of (3) with respect to y^i yields.

$$l_i^* = \left(\frac{1}{2}\frac{\beta^{\frac{1}{2}}}{L^{\frac{1}{2}}}\right) l_i + \left(1 + \frac{1}{2}\frac{L^{\frac{1}{2}}}{\beta^{\frac{1}{2}}}\right) b_i. \tag{6}$$

We know that

$$\frac{\partial l_i}{\partial y^j} = L^{-1} h_{ij}.$$

From the above relation

$$h_{ij}^* = \left(\frac{\beta}{2L}\right) A_0 h_{ij} + \frac{1}{4} A_0 \left(l_i b_j + l_j b_i\right) - \left(\frac{\beta}{4L}\right) A_0 l_i l_j - \left(\frac{L}{4\beta}\right) A_0 b_i b_j. \tag{7}$$

where

$$A_0 = 1 + \frac{\beta^{\frac{1}{2}}}{l^{\frac{1}{2}}}.$$

Theorem 2.1 (Angular Metric Tensor Transformation)

Under the transformation (3)

$$L^*(x, y) = (L^{1/2} + \beta^{1/2})(x, y)\,\beta^{1/2}(x, y).$$

the angular metric tensor (h^*_{ij}) of F^{*n} is given by (7) as follow:

$$h^*_{ij} = \left(\frac{\beta}{2L}\right)A_0 h_{ij} + \frac{1}{4}A_0\left(l_i b_j + l_j b_i\right) - \left(\frac{\beta}{4L}\right)A_0 l_i l_j - \left(\frac{L}{4\beta}\right)A_0 b_i b_j$$

where $A_0 = 1 + \frac{\beta^{\frac{1}{2}}}{l^{\frac{1}{2}}}.$

Further from equation (7) and $g_{ij} = h_{ij} + l_i l_j$ one gets

$$g^*_{ij} = \left(\frac{\beta}{2L}\right)A_0 g_{ij} + \frac{1}{2}U_0\left(l_i b_j + l_j b_i\right) - \left(\frac{\beta}{2L}\right)U_0 l_i l_j + U_1 b_i b_j \tag{8}$$

where $U_0 = 1 + \frac{3\beta^{\frac{1}{2}}}{2l^{\frac{1}{2}}}$

and $U_1 = 1 + \frac{3L^{\frac{1}{2}}}{2\beta^{\frac{1}{2}}}.$

Theorem 2.2. Under the transformation (3), the metric tensor of F^{*n} (g^*_{ij}) is described by (8).

From equation (8) and $C_{ijk} = \left(\frac{1}{2}\right)\frac{\partial g_{ij}}{\partial y^k}$,we get

$$C^*_{ijk} = \left(\frac{\beta}{2L}\right)A_0 C_{ijk} + \frac{1}{2}U_0\left(h_{ij}m_k + h_{jk}m_i + h_{ki}m_J\right) - \left(\frac{3L^{\frac{1}{2}}}{8\beta^{\frac{3}{2}}}\right)\left(m_I + m_J + m_K\right). \tag{9}$$

where $m_i = b_i - \left(\frac{\beta}{L}\right)l_i.$

Theorem 2.3. If the angular metric tensor h_{ij} of F^n vanishes, the torsion tensor of F^{*n} (C^*_{ijk}) also vanishes.

With the help of lemma (1) and relation

$$\sigma = \left(1 + \frac{\beta\rho}{L}\right),$$

we get

$$\frac{\partial\sigma}{\partial y^i} = \frac{\rho}{L}m_i. \tag{10}$$

From the definition of m_i, we get the following identities:

(i) $m_i l^i = 0,$

(ii) $m_i b^i = m_i m^i = b^2 - (\beta^2/L^2),$

(ii) $h_{ij} m^i = h_{ij} b^i = m_j$ and

(iv) $C^h_{ij} m_h = L^{-1}\rho\, h_{ij}.$ (11)

3. ϑ – Curvature Tensor

Definition 3.1. The v – curvature tensor $S_{h\,i\,j\,k}$ of $F^n = (M^n, L)$ with respect to Cartan's connection $C\Gamma$ is defined in [4] by

$$S_{hijk} = C_{hkm}C^m_{ij} - C_{hjm}C^m_{ik} \tag{12}$$

From (4), (8) and (11), we get

$$C^{*h}_{ij} = C^h_{ij} + R_1\left(h_{ij}m^k + h^k_j m_i + h^k_i m_j\right) - R_2\left(h_{ij}l^k R_3 + m_i m_j l^k\right) + \quad R_4\left(h_{ij}b^h R_3 + m_i m_j b^h\right). \tag{13}$$

where $R_1 = \left(\frac{3\beta}{2L}\right)\frac{\rho}{\sigma}$,

$$R_2 = \left(\frac{3(1-\sigma)\beta\rho}{L^2}\right)R_0\ ,$$

$$R_3 = \frac{\beta^{\frac{1}{2}}}{4l^{\frac{1}{2}}}\left(b^2 - \frac{\beta^2}{L^2}\right) + \sigma\ ,$$

$$R_4 = \left(\frac{\beta}{4L}\right)\rho R_0$$

and $R_0 = \frac{1}{\frac{\sigma\{(1-\sigma)\beta^2 - L^2\}}{L^2} - b^2}$.

From equation (9) and (13) ,we get

$$C^*_{hkm}C^*_{ij} = C_{hkm}C^h_{ij} + \mu_1 h_{ij}h_k + C_1 h_{hk}m_i m_j + C_2 h_{ij}m_h m_k + C_0\left(C_{ijk}m_h + C_{ijh}m_h + C_{ihk}m_j + C_{jhk}m_i\right)$$
$$+C_0^2 A_3\left(h_{jk}m_i m_h + h_{ih}m_j m_k + h_{jh}m_i m_k + h_{ik}m_j m_k\right) \tag{14}$$

where

$$\mu_1 = \left(b^2 - \frac{3\beta^2}{4L^2}\right)\left(\frac{\sigma\rho^2}{L^2}R_0 + \frac{\rho^2}{4L^2} + \frac{\rho^2}{4L^2}R_0\right) + \frac{\rho^2\sigma^2}{L^2}R_0,$$

$$C_0 = \frac{3\beta}{2L}\rho,$$

$$C_1 = \frac{\beta^2\rho^2}{4L^2}R_0(\sigma+1) + \frac{\beta^2\rho^2}{\sigma L^2}$$

and $C_2 = \frac{3\beta^2\rho^2}{4\sigma L^2} + \frac{\rho^2}{2L^2}R_0\left\{\sigma + \frac{1}{2}\left(b^2 - \frac{\beta^2}{L^2}\right)\right\}$.

Thus from (12) and (14) , we obtain the following

Theorem 3.1. (ϑ - Curvature Tensor Transformation)

Under the transformation (3) the v-curvature tensor $(S^*_{h\,i\,j\,k})$ of F^{*n} is written in the form

$$S^*_{hijk} = \sigma\left(\frac{\beta^{\frac{1}{2}}}{L^{\frac{1}{2}}}\right)s_{hijk} + \frac{3}{4\beta}h_{ij}e_{hk} + \frac{3L}{4}h_{hk}\left(e_{ij}+1\right) - \frac{L^{\frac{1}{2}}}{4\beta^{\frac{1}{2}}}h_{ik}e_{hj} - \frac{\beta^{\frac{1}{2}}}{4L^{\frac{1}{2}}}h_{hj}e_{ik}. \tag{15}$$

where $e_{ij} = \frac{1}{4}\mu_1 h_{ij} + \frac{3}{4}\mu_2 m_i m_j$

and $\mu_2 = \frac{3\beta^2\rho^2}{4L^2}R_0\left\{\sigma + \left(b^2 - \frac{\beta^2}{L^2}\right)\right\}$.

Theorem 3.2. The v - curvature tensor (S^{*}_{hijk}) of the transformed Finsler space F^{*n} vanishes if the angular metric tensor (h_{ij}) of F^n also vanishes, i. e. $S^{*}_{hijk} = 0$.

References

[1] Hashiguchi,M., Hojo,S. and Matsumoto,M.**(1973).**On Landsberg of two dimensions with (α, β) metric. *Jour. of Korean Math. Soc.* , **10**: 17-26.

[2] Kitayama, M. **(1998)**. Finslerian hypersurfaces and metric transformations, *Tensor*, **60**:171-178.

[3] Matsumoto, M. **(1985)**. The induced and intrinsic connection of a hypersurface and Finslerian projective geometry. *Jour. Math. Kyoto Univ.* , **25**: 107-144.

[4] Prasad, B. N. **(1990)**. On the torsion tensor R_{hijk} and P_{hijk} of Finsler spaces with a metric $ds = (g_{ij}(dx)\, dx^i dx^j)^{½} + b_i(x, y)\, dx^i$. *Indian Jour. Pure Appl. Math.*, **21(11)**: 27-39.

[5] Prasad,B. N. and Tripathi,B. K. **(2005).** Finslerian hypersurfaces and Kropina change of Finsler metric . *Journal of the Tensor Society of India*, **23**: 49-58.

[6] Rastogi, S. C. **(1989)**. On Finsler space with (α, β) metric. *Journal of Tensor Society of India* (JTSI), **7** :16 - 28.

[7] Shanker, G., Jangir, S., & Kaur, J. (**2022**). Curvatures on homogeneous Finsler spaces, arXiv. https://doi.org/10.48550/arXiv.2203.04667 (mathDG) ,**1**: 1-10

[8] Shibata,C. **(1978)**. On Finsler spaces with Kropina metric. *Reports on Mathematical Physics*,**13**:117-128.

[9] Shibata, C. , Singh,U.P. and Singh,A.K. **(1983)**. On induced and intrinsic theories of hypersurface of Kropina space. *Journal of Hokkaido Univ. of Education* (II A), **34**: 1-11.

[10] Singh, U. P. , B. N. Prasad, and Kumari,B. **(2003)**. On Kropina change of Finsler metric. *Tensor*, **64**: 181-188.

[11] Singh,U. P. and Srivastava, R.K. **(1992)**. On the h-transformation of some special Finsler spaces, *Indian Jour. of Pure & Applied. Math.*, **23(8)**: 555 - 559.

[12] Srivastava, A., **(2007)**. Generalized Kropina change of Finsler metric and Finslerian hypersurfaces. *Journal of the Tensor Society of India*, **1**: 97-106

[13] Srivastava, A., Miyan,Poonam . (**2011**). On Finslerian hypersurfaces given by generalized Kropina-type metric. *Bulletin of the Calcutta Mathematical Society*,**103**: 22-28.

□□

Nepal Journal of Mathematical Sciences (NJMS)
ISSN: **2738-9928 (*online*), 2738-9812 (*print*)**
Vol. 6, No. 1, 2025 (February): 7-20
DOI: 10.3126/njmathsci.v6i1.77369

Research Article
Received Date: February 10, 2025
Accepted Date: March 20, 2025
Published Date: April 8, 2025

Analysis of Foreign Exchange Rate Forecasting of Nepal using Long Short-Term Memory and Gated Recurrent Unit

Nissan Neupane[1] & Nawaraj Paudel[2*]

[1]*School of Mathematical Sciences, Tribhuvan University, Kirtipur, Kathmandu, Nepal*

[2]*Central Dept. of Computer Science and Information Technology, Tribhuvan University, Kathmandu, Nepal*

Corresponding Author: [*]nawarajpaudel@cdcsit.edu.np

Abstract: *Foreign exchange rate represents the value of one currency relative to another and influences international trade and investment. It is crucial for a country's economy as it affects the cost of imports and exports, impacting trade balances and inflation rates. This study compares the forecasting of the forex rate of Nepal and its volatility by using Long Short-Term Memory (LSTM) and Gated Recurrent Unit (GRU) models. The study uses secondary time series data that consists of foreign exchange rate from 2005 to 2024 A.D. Various error metrics were used to compare the performance of these models to predict the foreign exchange rate. The final result showed that the LSTM model outperformed GRU with superior forecasting accuracy, achieving a Mean Squared Error (MSE) of 4.7056, a Root Mean Squared Error (RMSE) of 2.1692, a Mean Absolute Error (MAE) of 2.0262, and a Mean Absolute Percentage Error (MAPE) of 1.5764%. In contrast, the GRU model yielded higher error metrics with an MSE of 7.1607, RMSE of 2.6759, MAE of 2.5673, and MAPE of 2.0061%. These findings highlight the effectiveness of LSTM in capturing historical trends and managing volatility, suggesting its robustness for forex rate prediction. Although the study focused on historical forex rates of the Nepalese Rupee against the US Dollar, incorporating additional economic indicators such as interest rates and Foreign Direct Investment (FDI) could enhance the model's predictive capabilities.*

Keywords: Forex rate, Long Short-Term Memory, Gated Recurrent Unit

1. Introduction

In today's globalized economy, the exchange rate between currencies plays a crucial role in shaping the economic landscape of a nation. The foreign exchange market is a global marketplace for exchanging national currencies against one another, and it is the largest and most liquid financial market in the world. Exchange rates fluctuate constantly due to various factors, including economic indicators, geopolitical events, and market speculation. For countries like Nepal, where the economy is significantly influenced by international trade and remittances, the exchange rate between the Nepalese Rupee and the US Dollar is particularly significant. This exchange rate impacts economy in multiple ways. Since Nepal is heavily dependent on imports, particularly from India and other countries where transactions are often denominated in USD, any fluctuations in the exchange rate can affect the cost of goods and services in the country. A depreciation of the NPR against the USD can lead to higher import costs, which may contribute to inflationary pressures within the domestic economy. Conversely, an appreciation of the NPR could make imports cheaper but might reduce the competitiveness of Nepalese exports, thereby affecting the trade balance. These dynamics underscore the importance of accurate forex rate forecasting, which can help policymakers, businesses, and investors make informed decisions [13].

Traditional forex forecasting methods like Autoregressive Integrated Moving Average and Vector Autoregression have been widely used, relying on historical data to identify trends. However, these linear models struggle to capture the non-linear relationships and complex dependencies typical in financial time series, limiting their forecasting accuracy [2].

In response to the limitations of traditional forecasting methods, the use of machine learning and deep learning techniques has gained significant attention in recent years. Machine learning models, particularly Neural Networks have shown great potential in forecasting complex time series data. GRU networks are a type of Recurrent Neural Network which use gating mechanisms to control the flow of information, helping to overcome the issues of exploding gradients commonly encountered in traditional RNNs. GRUs are particularly valuable for tasks such as time series forecasting and financial predictions, where capturing historical dependencies can significantly improve accuracy [4]. LSTM networks, another type of Recurrent Neural Network, are designed to address the problem of long-term dependencies in time series data. Traditional RNNs struggle with the vanishing gradient problem, where the gradients used to update the weights of the network become extremely small, leading to difficulties in learning long-term dependencies. LSTMs overcome this issue by introducing memory cells and gates that control the flow of information, allowing the network to retain important information over long sequences and thus providing more accurate forecasts [9]. The application of LSTM and GRU models to forex rate forecasting has been explored in various studies with promising results. Authors in [1] suggested that LSTM and Artificial Neural Network are the most commonly used machine learning algorithms for forex market. Similarly, authors in [7] highlighted the effectiveness of LSTM networks in financial forecasting, noting their ability to model the sequential nature of time series data more effectively than traditional models. Despite extensive research on machine learning, limited work has focused on emerging markets like Nepal. Most studies target developed economies with different data and market conditions. This study addresses that gap by comparing LSTM and GRU models in forecasting Nepal's USD/NPR exchange rate.

1.1. Research Questions

The specific research question that is addressed is as follows:

- How do LSTM and GRU models forecast foreign exchange rate of Nepalese Rupee against US Dollar?
- What is the comparative performance of LSTM and GRU models in predicting the Nepalese Rupee against US Dollar?

1.2. Research Objectives

The objectives of this study are:

- To develop and implement LSTM and GRU models for forecasting Nepalese Rupee against US Dollar.
- To evaluate and compare the prediction performance of LSTM and GRU models in forecasting Nepalese Rupee against US Dollar.

2. Literature Review

Over the years, various models and approaches have been developed to predict exchange rate movements, ranging from traditional economic theories such as purchasing power parity (PPP) and interest rate parity (IRP) to more advanced econometric and machine learning techniques. Early studies, such as those by [10], challenged the predictive power of fundamental models, emphasizing the superiority of random walk behavior. Since then, researchers have explored time series models, artificial intelligence, and hybrid approaches to improve forecasting accuracy. Despite these advancements, exchange rate prediction remains a complex and debated field due to the influence of multiple economic, political, and speculative factors. Numerous experiments have been carried out over time to forecast foreign exchange rate using different machine learning methods. This literature review examines key theoretical frameworks, empirical findings, and emerging methodologies in foreign exchange rate forecasting, identifying trends and gaps in the existing research.

Authors in [6] built an effective model for predicting forex price trends by leveraging Recurrent Neural Networks (RNNs), with a particular focus on LSTM networks. This research utilized secondary data comprising historical forex prices from several financial markets over an extended period. The data was meticulously preprocessed and divided into a training set and a testing set, following the standard approach of assigning 70% to training and 30% to testing. The performance of the model was evaluated using Mean Squared Error (MSE) and Mean Absolute Error (MAE) as key metrics. The LSTM model achieved an MSE value of 0.003052 and a MAE of 0.002390. Based on these findings, the study recommended the use of LSTM networks for forex price trend forecasting in financial institutions and trading firms as LSTM is superior to traditional methods for forecasting forex price trends. Additionally, the comparative analysis of traditional statistical methods with modern machine learning techniques provided a comprehensive evaluation of the models' performance, highlighting the advantages of using RNNs for time series forecasting. The study also contributed to the growing body of literature on the application of deep learning techniques in finance, demonstrating the practical benefits of these methods in enhancing prediction accuracy. The detailed analysis and comparison of various models ensured that the study's conclusions were well-rounded and supported by empirical evidence.

Yildirim et al. explored the use of LSTM models for forecasting the directional movement of the EUR/USD currency pair over different time horizons, specifically one day, three days, and five days ahead. The study introduced a novel performance metric, profit_accuracy, to evaluate the effectiveness of the predictions in generating profitable transactions. The data included both macroeconomic indicators and technical indicators, which were used to train and evaluate the LSTM models. The research applied two separate LSTM models, one trained using macroeconomic data (ME_LSTM) and the other using technical indicators (TI_LSTM). A classifier was developed to determine the directional movement of the EUR/USD pair into three classes: no_action, decrease, and increase. The hybrid model, which combined both macroeconomic and technical indicator features (ME_TI_LSTM), was also tested. The study found that the ME_LSTM model slightly outperformed the TI_LSTM model in terms of both profit_accuracy and the number of transactions generated, though the difference was minimal and statistically insignificant. The hybrid model (ME_TI_LSTM), which combined all features, did not show a significant improvement in accuracy compared to the individual models. However, the proposed hybrid model demonstrated the best overall performance, achieving an average profit_accuracy of 73.61% across all prediction periods. It also reduced the number of transactions by 40.37% on average compared to the baseline models, primarily by dropping risky transactions. In conclusion, the study provided compelling evidence that the hybrid LSTM model offers a robust approach to forecasting the directional movement of the EUR/USD currency pair [15].

Authors in [12] explored the effectiveness of LSTM networks, particularly when combined with event-driven inputs, for predicting foreign exchange rates. The study focused on developing a model that could leverage both the sequential patterns inherent in time series data and the impact of specific events, which often cause significant fluctuations in forex markets. The data utilized in this research consisted of historical forex rates and event data over a substantial period, including major economic announcements, geopolitical events, and other news that could influence forex prices. The LSTM model was constructed, incorporating event-driven features to enhance its predictive capabilities. The hybrid approach aimed to address the limitations of traditional LSTM models, which may not fully capture the impact of sporadic, yet significant events on forex prices. The study's results demonstrated that the event-driven LSTM model significantly improved the accuracy of forex price predictions compared to standard LSTM models and other traditional methods. The performance of the model was evaluated using metrics such as Root Mean Error (RME), Root Mean Squared Error (RMSE), Mean Absolute Error (MAE), and Mean Absolute Percentage Error (MAPE). The event-driven LSTM achieved an RME of 0.006*10^(-3), RMSE of 2.407*10^(-3), MAE of 1.708*10^(-3), and MAPE of 0.194% highlighting its effectiveness in capturing the complex, event-driven patterns within the forex market.

Authors in [11] explored the effectiveness of combining Perceptron with Genetic Algorithms (GAs) for predicting foreign exchange rates. The study focused on developing a hybrid model that leverages the strengths of both techniques. The data utilized in this research consisted of historical forex rates from multiple currency pairs over a substantial period. The hybrid model aimed to enhance prediction accuracy by addressing the limitations of individual methods. The results demonstrated that the hybrid Perceptron-GA model significantly improved the accuracy of forex rate predictions compared to traditional methods and standalone Perceptron models. The evaluation of model performance was based on metrics such as Mean Squared Error (MSE) and Mean Absolute Error (MAE). The hybrid model achieved an MSE of 0.01 and a MAE of 0.0082. This result underscored the effectiveness of integrating Perceptron and GAs in capturing the complex, non-linear patterns inherent in forex data. One of the key strengths of this study was its innovative approach to combining machine learning and evolutionary algorithms to tackle a real-world financial problem. The research also contributed to the broader field of financial forecasting by demonstrating the potential of hybrid models in enhancing prediction accuracy. The focus on optimizing neural networks using evolutionary algorithms added a new dimension to the existing literature, showcasing the practical benefits of this approach in finance.

Authors in [14] investigated the effectiveness of tree ensemble methods, including Random Forests, Gradient Boosting Machines (GBMs), and Extreme Gradient Boosting (XGBoost), for predicting trends in the forex market. The study utilized historical forex rate data spanning multiple currency pairs over a significant time period. The results of the study indicated that XGBoost significantly outperformed traditional methods and simpler machine learning models in predicting forex market trends. The performance of the models was evaluated using metrics such as Mean Squared Error (MSE) and Mean Absolute Error (MAE), with XGBoost achieving MSE of 0.009 and MAE of 0.0075. These results underscored the models' ability to handle the intricacies of forex data, making them highly effective for trend prediction. The research also contributed to the broader field of financial forecasting by demonstrating the effectiveness of tree ensemble methods in capturing complex patterns in forex data.

Despite the importance of exchange rate fluctuations for Nepal's economy, little research has focused on forecasting forex rates in the Nepalese context. Most studies target developed countries, with limited use of advanced machine learning methods. This study aims to fill that gap by applying and comparing GRU and LSTM models to predict the Nepali Rupee exchange rate, identifying which model offers better forecasting accuracy.

3. Methodology

Forecasting foreign exchange rates involves predicting the value of one currency relative to another. Accurate predictions are crucial for various stakeholders, including investors, businesses engaged in international trade, and policymakers. Effective forecasting helps in managing currency risk, optimizing investment strategies, and implementing sound economic policies [3]. In Nepal, which has a significant reliance on remittances and international trade, precise forex rate forecasts are vital for maintaining economic stability and improving growth. The analysis of forecasting forex rates in Nepal using LSTM and GRU models is rooted in the intersection of financial forecasting and advanced machine learning techniques. Accurate prediction of forex rates is essential for effective financial decision-making, economic planning, and risk management. This study focuses on applying two advanced machine learning models: LSTM and GRU to forecast the forex rate of Nepal in relation to major currency such as USD.

3.1. Data Collection

The dataset used in this study consists of time series data encompassing historical records relevant to forex rates. This data is sourced from secondary sources, specifically from the Nepal Rastra Bank. The time series dataset includes historical forex rate information from 2005 to 2024 that provides insights into past currency fluctuations, which is essential for evaluating the forecasting capabilities of the LSTM and GRU models. This historical data provides the foundation for evaluating the forecasting performance of the LSTM and GRU models. The data includes time series records of forex rates between the Nepalese Rupee and major currency, the US Dollar.

3.2. Stationarity Test

For an accurate forecasting of a time series forecasting, a key concept is stationarity. Stationarity in the context of time series data refers to the property of a time series where its statistical properties, such as mean, variance, and autocorrelation, remain constant. For time series data to be stationarity, it should not exhibit trends, seasonality, or other time-dependent structures that cause its statistical properties to change over time. When the data is stationary, it is easier to model and forecast future values, as the past behavior of the time series can be used to predict future behavior. The Augmented Dickey-Fuller test is a parametric method used to assess whether a unit root is present in a dataset. The existence of a unit root suggests that the data is non-stationary, indicating that it may display a trend or seasonal pattern. To perform the ADF test, an autoregressive model with a differencing term is fitted to the data, and the significance of the differencing coefficient is evaluated.

Table 1. Augmented Dickey-Fuller Test

Variables	Dickey-Fuller	Lag order	p-value	Stationarity
Actual Forex Rate	-2.9564	0	0.1732(>0.05)	Non-stationary
1^{st} order difference	-16.0064	1	0.0100(<0.05)	Stationary

The table 1 summarizes the results of the ADF test applied to the actual forex rate and its first-order difference to determine stationarity. For the actual forex rate, the Dickey-Fuller test statistic is -2.95645431195, with a lag order of 0. The corresponding p-value is 0.173228, which is greater than the significance level of 0.05. This result indicates that the null hypothesis of a unit root cannot be rejected, suggesting that the actual forex rate series is non-stationary. In contrast, when the first-order difference of the forex rate is tested, the Dickey-Fuller test statistic is -16.0064402294 with a lag order of 1. The p-value for this test is 0.010, which is significantly less than 0.05. This implies that the null hypothesis of a unit root is rejected, indicating that the first-order differenced series is stationary. Therefore, while the original forex rate series exhibits non-stationarity, differencing the series once renders it stationary, which is essential for further time series analysis and forecasting.

3.3. Data Preprocessing and Splitting

The collected data was cleaned to address any inconsistencies or missing values. This included handling outliers, correcting data entry errors, and interpolating missing values where necessary to ensure a complete and accurate dataset. The data was then transformed to make it suitable for analysis using normalization and feature engineering. Normalization was done for scaling the data to a uniform range to improve the performance and convergence of the models. Min-Max scaling technique was applied for normalization. Feature engineering was done for creating relevant features from the raw data that can enhance the predictive capability of the models. This includes lag variables, and moving averages. The dataset was divided into training and test subsets using an 80-20 split ratio. This division allows for robust model training and evaluation, helping to assess the model's performance on unseen data.

3.4. Model Description

Long Short-Term Memory (LSTM) is a type of recurrent neural network (RNN) designed to address the limitations of traditional RNNs, particularly the vanishing gradient problem. Proposed by [9], LSTMs are highly effective in capturing long-term dependencies in sequential data, making them well-suited for time series forecasting tasks such as foreign exchange rate prediction. Unlike standard RNNs, LSTMs incorporate specialized gating mechanisms – the forget gate, input gate, and output gate – which regulate the flow of information through the network. These gates enable LSTMs to retain relevant historical data while discarding irrelevant information, leading to improved predictive performance in highly volatile financial markets. Due to their ability to model complex temporal relationships, LSTMs have been widely applied in financial time series forecasting, demonstrating superior accuracy compared to traditional econometric models like ARIMA and GARCH [7]. By capturing both short-term and long-term dependencies, LSTMs are highly effective for tasks like time series forecasting, where the future values depend on a complex and non-linear relationship with past observations [8]. The different equations of LSTM are as follows.

$f_t = \sigma(W_f \,.\, [h_{t-1}, x_t] + b_f)$ Forget gate

$i_t = \sigma(W_i \,.\, [h_{t-1}, x_t] + b_i)$ Input gate

$\tilde{C}_t = tanh(W_C \,.\, [h_{t-1}, x_t] + b_C)$ Candidate cell state

$C_t = f_t * C_{t-1} + i_t * \tilde{C}_t$ Update cell state

$o_t = \sigma(W_o \,.\, [h_{t-1}, x_t] + b_o)$ Output gate

$h_t = o_t * \tanh(C_t)$ Hidden state update

GRU is a variant of recurrent neural networks (RNNs) introduced by [4] to address the vanishing gradient problem and improve sequence modeling efficiency. Similar to LSTM, GRU is designed to capture long-term dependencies in sequential data, making them suitable for time series forecasting tasks such as foreign exchange rate prediction. However, GRUs have a simpler architecture than LSTMs, as they use only two gates – the reset gate and update gate – instead of three. This reduction in complexity allows

GRUs to achieve comparable performance with LSTMs while being more computationally efficient [5]. Recent studies have demonstrated the effectiveness of GRU-based models in financial forecasting, showing their ability to adapt to the nonlinear and volatile nature of exchange rate movements. Given their efficiency and accuracy, GRUs have become a popular alternative to LSTMs in deep learning applications for time series analysis. The different equations of GRU are as follows.

$r_t = \sigma(W_r . [h_{t-1}, x_t] + b_r)$ Reset gate

$z_t = \sigma(W_z . [h_{t-1}, x_t] + b_z)$ Update gate

$\tilde{h}_t = tanh(W_h . [r_t * h_{t-1}, x_t] + b_h)$ Candidate hidden state

$h_t = (1 - z_t) * h_{t-1} + z_t * \tilde{h}_t)$ Reset gate

3.5. Experimental Setup

Both LSTM and GRU algorithms were implemented using Python Programming Language and the libraries such as Keras, Pandas, NumPy, and Matplotlib. The models underwent training and testing on Microsoft Windows 11, AMD Ryzen 5 5500U CPU @ 2.10 GHz, and 8 GB RAM.

3.6. Performance Evaluation

The performance of both LSTM and GRU models are assessed using Mean Squared Error (MSE), Root Mean Squared Error (RMSE), Mean Absolute Error (MAE), and Mean Absolute Percentage Error (MAPE). MSE quantifies the average squared difference between the predicted values and the actual values. It helps to evaluate how well a model performs. A lower MSE indicates a better model.

$$MSE = \frac{1}{n}\sum_{i=1}^{n}(y_i - \hat{y}_i)^2 \qquad (1)$$

RMSE measures the average magnitude of errors by taking the square root of the MSE. This metric expresses the error in the same units as the predicted values, which makes it easier to interpret compared to MSE. It penalizes large errors more than small ones. Lower RMSE values indicate that the model's predictions are closer to the actual values, and the model has fewer and smaller errors overall.

$$RMSE = \sqrt{MSE} \qquad (2)$$

MAE measures the average absolute difference between actual and predicted values. It provides a straightforward interpretation of how far predictions are from actual values. It is less sensitive to outliers compared to MSE and RMSE. It expresses the error in the same unit as the original data, making it easy to interpret. A lower MAE indicates a more accurate model.

$$MAE = \frac{1}{n}\sum_{i=1}^{n}|y_i - \hat{y}_i| \qquad (3)$$

MAPE evaluates the accuracy of the model's predictions as a percentage of the actual values. This metric provides a relative measure of error, making it useful for comparing the performance of different forecasting models or datasets. MAPE calculates the average percentage by which the predicted values deviate from the actual values. A lower MAPE indicates that the model's forecasts are more accurate in percentage terms, giving a clear understanding of prediction accuracy relative to the size of the actual values.

$$MAPE = \frac{1}{n}\sum_{i=1}^{n}\left|\frac{y_i - \hat{y}_i}{y_i}\right| \times 100 \qquad (4)$$

4. Result Analysis

The Figure 1 presents the historical trend of the Nepalese rupee against the US dollar over a period of days. The chart reveals a steady upward movement in the forex rate, showing a gradual appreciation of the Nepalese rupee against the US dollar. A notable point in the chart is the period of increased volatility, which occurs around the earlier days, particularly between days 3000 and 3500. This fluctuation suggests that there were significant market events or interventions influencing the exchange rate during that time. From day 3500 onward, the chart shows a consistent increase in the forex rate with only occasional small fluctuations. The general upward trend implies a gradual depreciation of the Nepalese rupee, indicating that more units of the rupee are needed to purchase one US dollar as time progresses.

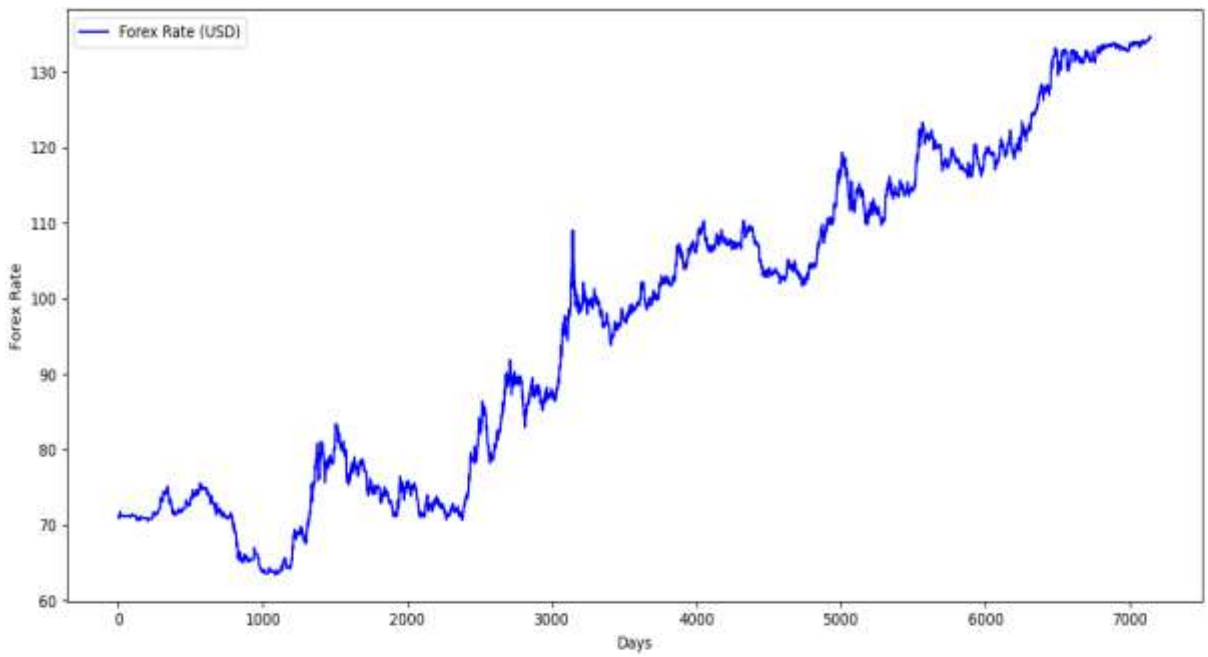

Figure 1. Trendline of Forex Rate of Nepal (2005-2024)

4.1. Analysis of LSTM

The Figure 2 illustrates the training loss of LSTM model over 100 epochs. The vertical axis represents the loss value, which quantifies the difference between the predicted and actual values during training, while the horizontal axis shows the number of epochs. The chart indicates a rapid decrease in the training loss within the first few epochs, with the loss value dropping sharply from above 0.52 to around 0.48 within the first 5 epochs. After this initial decline, the training loss plateaus and stabilizes, maintaining a relatively constant value just below 0.48 for the remainder of the training process up to 100 epochs.

The pattern shows that the model learns quickly during the initial training phase, with a steep loss decline. After that, further training offers minimal improvement, suggesting diminishing returns. This stabilization indicates the model has minimized error, and additional training may lead to overfitting without significant gains.

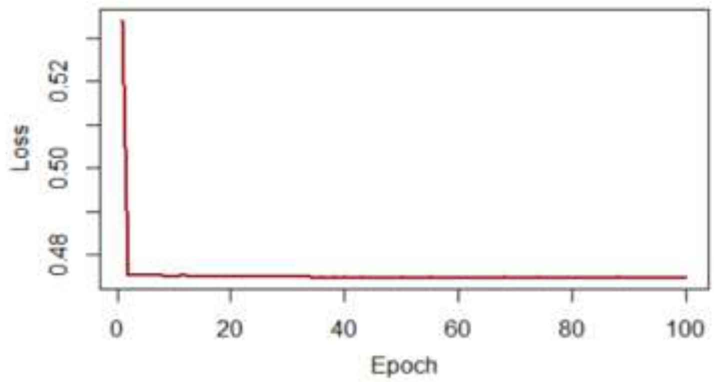

Figure 2. Training Loss of LSTM

Table 2. Summary Result of LSTM Model

Input Feature	**Metrics**			
Unit	**MSE**	**RMSE**	**MAE**	**MAPE**
30	7.0025	2.6462	2.4719	1.9225%
40	5.3176	2.3059	2.1393	1.6623%
50	4.7056	2.1692	2.0262	1.5764%
60	4.9369	2.2219	2.1189	1.6547%

The Table 2 provides a detailed comparison of the performance metrics for testing dataset of LSTM with varying numbers of unit while maintaining the same epoch count of 50, batch size of 64, and dropout rate of 0.3. The models differ only in the number of LSTM units, and their performance is evaluated using four metrics: Mean Squared Error (MSE), Root Mean Squared Error (RMSE), Mean Absolute Error (MAE), and Mean Absolute Percentage Error (MAPE).

For the LSTM model with 30 units, the MSE is 7.0025, indicating the average squared difference between actual and predicted values. The RMSE, which translates this into the same units as the data, is 2.6462, providing a tangible measure of the prediction error. The MAE is 2.4719, representing the average absolute magnitude of prediction errors, and the MAPE is 1.9225%, suggesting a relatively low prediction error as a percentage of the actual values. When the number of units is increased to 40, the model shows improved performance across all metrics. The MSE decreases to 5.3176, and the RMSE to 2.3059, reflecting a reduced prediction error. Similarly, the MAE drops to 2.1393, and the MAPE to 1.6623%, indicating better accuracy and robustness in predictions. The model with 50 units continues this trend, achieving the lowest overall MSE of 4.7056, RMSE of 2.1692, MAE of 2.0262, and MAPE of 1.5764% among all models. These metrics suggest this model provides the most accurate and reliable predictions within this setup. However, increasing the number of units to 60 slightly increases the errors, with an MSE of 4.9369, RMSE of 2.2219, MAE of 2.1189, and MAPE of 1.6547%. While still competitive, this model demonstrates that adding more units does not always lead to better performance, potentially due to diminishing returns in predictive accuracy.

Among all the models evaluated, the LSTM model with 50 units demonstrates the best overall performance, achieving the lowest error metrics. This indicates that the configuration with 50 units is optimal for balancing complexity and predictive accuracy for the forecasting of forex rate of Nepal.

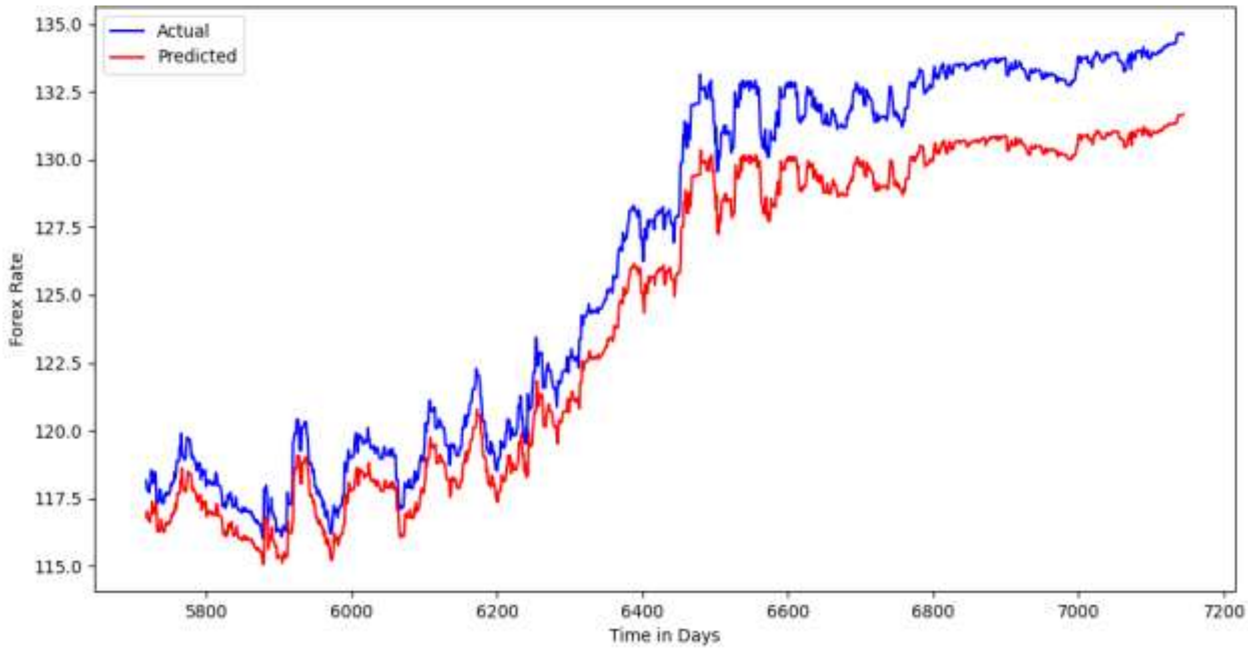

Figure 3. Actual Vs Predicted Forex Rate of LSTM

The Figure 3 illustrates the performance of the testing dataset for the best-performing Long Short-Term Memory (LSTM) model, identified as the LSTM model trained with 50 units. The blue line represents the actual forex rates, while the red line depicts the predicted forex rates generated by the model. From the figure, it is evident that the model closely follows the actual forex rates over time, particularly in the earlier stages, where the blue and red lines are nearly overlapping. This close alignment demonstrates the model's ability to effectively learn and replicate the trends and patterns present in the historical data.

As the time progresses, however, there is a noticeable divergence between the actual and predicted values, particularly in the latter part of the dataset. This gap suggests that while the model is highly accurate, it may face challenges in fully capturing the more volatile or less predictable fluctuations in forex rates in these later periods.

Overall, the small differences between the actual and predicted values align with the previously discussed performance metrics, such as the low Mean Squared Error (MSE), Root Mean Squared Error (RMSE), Mean Absolute Error (MAE), and Mean Absolute Percentage Error (MAPE). These metrics underscore the model's robustness and accuracy in forecasting forex rates, making it a reliable tool for time series predictions in scenarios requiring precision, such as currency exchange rate forecasting.

4.2. Analysis of GRU

The Figure 4 illustrates the training loss of an GRU model as a function of the number of epochs during the training process. The vertical axis represents the loss, while the horizontal axis shows the number of epochs, ranging from 0 to 70. The chart indicates that the training loss starts relatively high at the beginning of the training. However, it rapidly decreases within the first few epochs, which is a common pattern indicating that the model is quickly learning the key patterns in the data. After about 10 to 20 epochs, the loss begins to stabilize, approaching a value close to zero.

This flattening of the curve suggests that the model has reached a point where further training brings minimal improvements in reducing the loss, indicating convergence. The steady loss value towards the end of the epochs indicates that the model has effectively learned from the training data, and additional epochs are unlikely to significantly improve its performance. This suggests that the training process is efficient and that the chosen number of epochs is sufficient for the model to achieve optimal performance without overfitting.

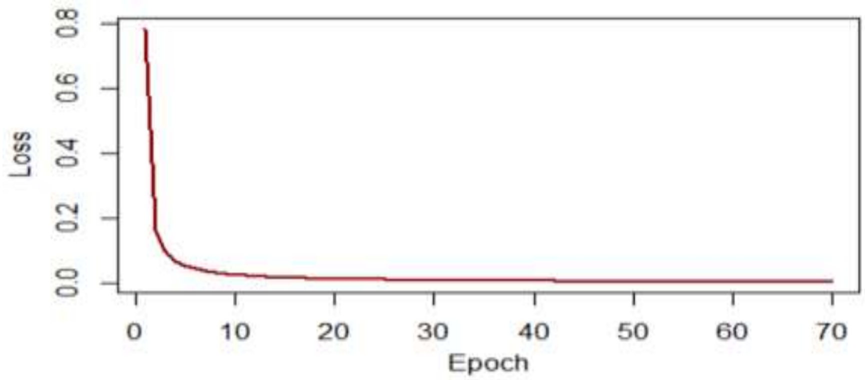

Figure 4. Training Loss of GRU

Table 3. Summary Result of GRU Model

Input Feature	**Metrics**			
Unit	**MSE**	**RMSE**	**MAE**	**MAPE**
30	20.4508	4.5222	4.4064	3.4539%
40	11.5716	3.4017	3.2905	2.5753%
50	7.1607	2.6759	2.5673	2.0065%
60	8.3174	2.8839	2.8074	2.2012%

The Table 3 provides a detailed comparison of the performance metrics for the testing dataset of Gated Recurrent Unit (GRU) models with varying numbers of units, while maintaining a constant epoch count of 50, batch size of 64, and dropout rate of 0.3. The models are evaluated using four metrics: Mean Squared Error (MSE), Root Mean Squared Error (RMSE), Mean Absolute Error (MAE), and Mean Absolute Percentage Error (MAPE).

For the GRU model with 30 units, the MSE is 20.4508, which is relatively high compared to the other configurations. This translates into an RMSE of 4.5222, indicating a significant prediction error in the same units as the data. The MAE is 4.4064, reflecting the average magnitude of prediction errors, while the MAPE of 3.4539% suggests a moderate percentage error relative to the actual values. Increasing the number of units to 40 leads to substantial improvements in performance. The MSE decreases to 11.5716, and the RMSE to 3.4017, showing a notable reduction in prediction error. Similarly, the MAE drops to 3.2905, and the MAPE to 2.5753%, indicating enhanced accuracy and better trend-capturing capability. The model with 50 units achieves the best overall performance, with the lowest MSE of 7.1607, RMSE of 2.6759, MAE of 2.5673, and MAPE of 2.0065%. These metrics confirm that this configuration provides the most accurate and reliable predictions for the testing dataset. However, increasing the number of units to 60 slightly worsens the performance, as evidenced by an MSE of 8.3174, RMSE of 2.8839, MAE of 2.8074, and MAPE of 2.2012%. This suggests that adding more units beyond a certain point may lead to diminishing returns, possibly due to an increase in model complexity without corresponding gains in predictive accuracy.

Among the GRU models evaluated, the configuration with 50 units stands out as the optimal choice, achieving the lowest error metrics across all categories. This indicates that the model with 50 units strikes the best balance between complexity and accuracy, making it the most effective for forecasting tasks in this scenario.

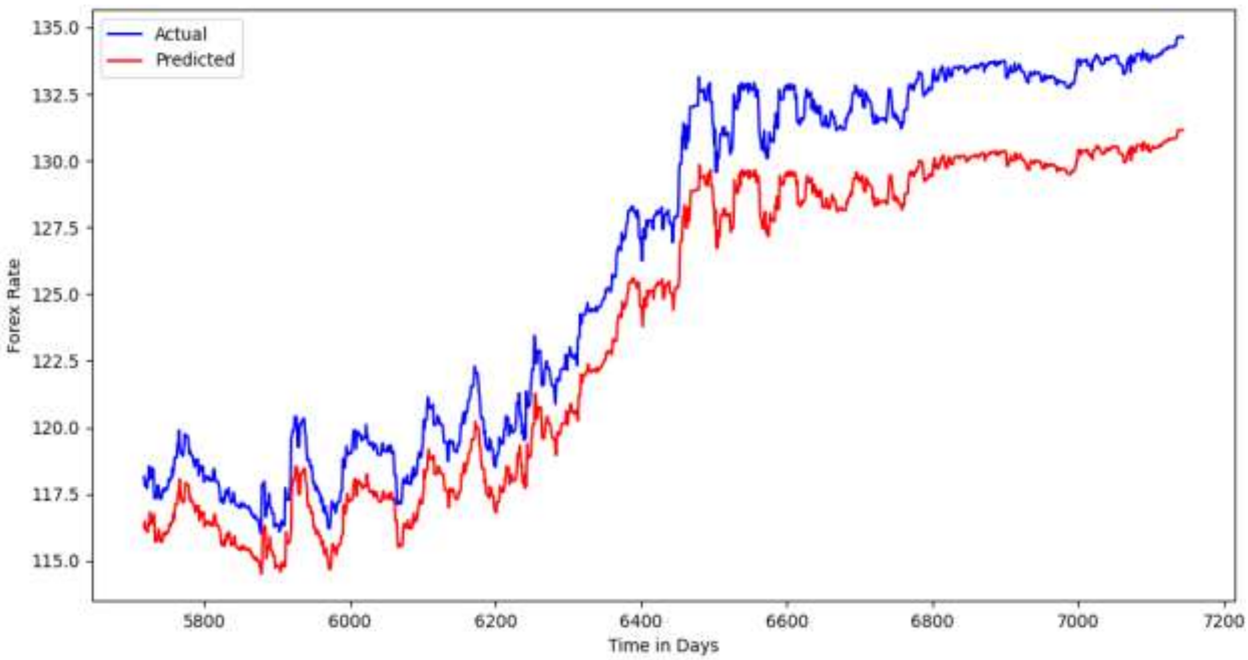

Figure 5. Actual Vs Predicted Forex Rate of GRU

The Figure 5 illustrates the performance of the testing dataset for the best-performing GRU model, identified as the GRU model trained with 50 units. The blue line represents the actual forex rates, while the red line depicts the predicted forex rates generated by the model. From the figure, it is clear that the model closely tracks the actual forex rates over time, especially in the earlier segments where the blue and red lines almost overlap. This alignment highlights the model's capability to accurately capture the underlying trends and patterns in the historical data, showcasing its predictive strength.

However, as time progresses, a slight divergence between the actual and predicted values becomes apparent, particularly in the latter stages of the dataset. This gap indicates that while the model performs exceptionally well overall, it encounters some difficulty in fully capturing the more volatile or less predictable fluctuations in forex rates toward the end of the time series.

The small differences between the actual and predicted values reflect the previously discussed performance metrics, such as the low Mean Squared Error (MSE), Root Mean Squared Error (RMSE), Mean Absolute Error (MAE), and Mean Absolute Percentage Error (MAPE). These metrics confirm the model's robustness and accuracy in forecasting forex rates, making it a reliable tool for time series predictions in practical applications like currency exchange rate forecasting.

4.3. Model Comparison

This research focuses on identifying the most accurate and reliable model for predicting forex rates. To achieve this, best-performing versions of each Long Short-Term Memory and Gated Recurrent Unit models are selected for comparison. These versions are chosen based on their superior performance metrics, such as Mean Squared Error (MSE), Root Mean Squared Error (RMSE), Mean Absolute Error (MAE), and Mean Absolute Percentage Error (MAPE). By focusing on these top-performing models, the comparison aims to determine which architecture: LSTM or GRU offers the most effective and precise predictions for the given data and task.

Table 4. Model Comparison

Model	**Metrics**			
	MSE	**RMSE**	**MAE**	**MAPE**
LSTM	4.7056	2.1692	2.0262	1.5764%
GRU	7.1607	2.6759	2.5673	2.0065%

The Table 4 presents a comparative analysis of two models, LSTM and GRU, using four evaluation metrics: Mean Squared Error (MSE), Root Mean Squared Error (RMSE), Mean Absolute Error (MAE), and Mean Absolute Percentage Error (MAPE). The MSE value of the LSTM model is 4.7056, which indicates that average squared difference between the predicted and actual values, compared to MSE of 7.1607 for GRU model. The RMSE value of the LSTM model is 2.1692, which measures the squared root of average squared difference between predicted values, compared to RMSE of 2.6759 for GRU. The average absolute difference between the predicted and actual values of LSTM model is 2.0262 compared to that of 2.5673 of GRU model. The MAPE value of 1.5764% of LSTM model means that the average difference between the forecasted value and the actual value is 1.5764% compared to that of 2.0065% of GRU model. Lower values of MSE, RMSE, MAE, and MAPE indicate better model performance. Thus, LSTM model outperforms GRU model in all four of the metrics for forecasting the forex rate of Nepal.

5. Conclusion

This study employed historical data of forex rate of Nepali Rupee against US dollar. The Augmented Dickey-Fuller (ADF) test was employed to assess stationarity. The result showed that the actual forex rate was non-stationary (p-value = 0.173228 > 0.05). However, after first-order differencing, the series becomes stationary (p-value = 0.010 < 0.05). Based on the ADF test results, a lag of 1 was chosen for model computations. The dataset was split into training (80%) and testing (20%) subsets. Min-Max scaling was applied to normalize the features, ensuring all features contribute equally and improving the convergence of learning algorithms. Both LSTM and GRU models were implemented using Python programming language. The best performance was achieved by the LSTM model with 50 units, showing the MSE of 4.7056, RMSE of 2.1692, MAE of 2.0262, and MAPE of 1.5764%. Similarly, the best performance was observed in the GRU model with 50 units, with the lowest MSE of 7.1607, RMSE of 2.6759, MAE of 2.5673, and MAPE of 2.0065%. The analysis demonstrated that the LSTM model significantly outperformed the GRU model in accuracy and precision, as shown by lower MSE, RMSE, MAE, and MAPE metrics. The LSTM model's superior ability to capture historical trends and handle time series data with minimal error highlighted its robustness in forecasting volatile exchange rates. The findings indicated that the LSTM model is more effective in predicting the forex rate of Nepal. Given the ability of LSTM model to effectively capture historical trends and handle time series data with minimal error, it is recommended to use LSTM models for forecasting the forex rate of Nepal.

Although the study focused on historical forex rates of NPR against US Dollar, incorporating additional economic indicators such as interest rates, Foreign Direct Investment (FDI) etc. could further enhance the model’s predictive capabilities. The collaboration between academic institutions, financial organizations, and government bodies should be encouraged to promote the use of advanced forecasting techniques for forex forecasting.

References

[1] Ayitey Junior, M., Appiahene, P., Appiah, O., & Bombie, C. N. **(2023)**. Forex market forecasting using machine learning: Systematic Literature Review and meta-analysis. *Journal of Big Data*, **10(9):**.

[2] Box, G. E. P., Jenkins, G. M., & Reinsel, G. C. **(2008)**. Time Series Analysis: Forecasting and Control. In *Time Series Analysis: Forecasting and Control,* (4th ed.). Wiley.

[3] Cheung, Y. W., & Chinn, M. D. **(2001)**. Currency traders and exchange rate dynamics: A survey of the US market. *Journal of International Money and Finance*, **20(4)**.

[4] Cho, K., van Merrienboer, B., Gulcehre, C., Bahdanau, D., Bougares, F., Schwenk, H., & Bengio, Y. **(2014)**. *Learning Phrase Representations using RNN Encoder-Decoder for Statistical Machine Translation*.

[5] Chung, J., Gulcehre, C., Cho, K., & Bengio, Y. **(2014)**. *Empirical Evaluation of Gated Recurrent Neural Networks on Sequence Modeling*.

[6] Dobrovolny, M., Soukal, I., Lim, K. C., Selamat, A., & Krejcar, O. **(2020)**. Forecasting of FOREX Price Trend using Recurrent Neural Network - Long short-term memory. *Proceedings of the International Scientific Conference Hradec Economic Days 2020*, **10**.

[7] Fischer, T., & Krauss, C. **(2018)**. Deep learning with long short-term memory networks for financial market predictions. *European Journal of Operational Research*, **270(2)**: 654–669.

[8] Greff, K., Srivastava, R. K., Koutnik, J., Steunebrink, B. R., & Schmidhuber, J. **(2017)**. LSTM: A Search Space Odyssey. *IEEE Transactions on Neural Networks and Learning Systems*, **28(10)**.

[9] Hochreiter, S., & Schmidhuber, J. **(1997)**. Long Short-Term Memory. *Neural Computation*, ***9*(8)**.

[10] Meese, R. A., & Rogoff, K. **(1983)**. Empirical exchange rate models of the seventies: Do they fit out of sample? *Journal of International Economics*, **14(1)**: 3–24.

[11] Meirinaldi, Yolanda, & Seputra, Y. E. A. **(2022)**. Analysis of Foreign Exchange Using Perceptron and Genetic Algorithm Machine Learning (GALM). *European Journal of Business and Management Research*, **7(6)**.

[12] Qi, L., Khushi, M., & Poon, J. **(2020)**. Event-Driven LSTM for Forex Price Prediction. *2020 IEEE Asia-Pacific Conference on Computer Science and Data Engineering (CSDE)*.

[13] Shrestha, M. B., & Chaudhary, R. K. **(2012)**. The impact of exchange rate fluctuations on exports: A case study of Nepal. *Journal of International Economics and Economic Policy*, **9(1)**: 79–90.

[14] Thao, N., Nguyen, H.-C., Mach, B.-N., Thuan, D., Quynh, T., Huong, T., Chi, D., & Nguyen, T. **(2024)**. *Unlocking Forex Market Trends: Advanced Predictive Modeling with Tree Ensembles*.

[15] Yıldırım, D. C., Toroslu, I. H., & Fiore, U. **(2021)**. Forecasting directional movement of Forex data using LSTM with technical and macroeconomic indicators. *Financial Innovation*, **7(1)**.

Nepal Journal of Mathematical Sciences (NJMS)
ISSN: **2738-9928** (*online*), **2738-9812** (*print*)
Vol. 6, No. 1, 2025 (February): **21-34**
DOI: 10.3126/njmathsci.v6i1.77372

Research Article
Received Date: January 5, 2025
Accepted Date: March 25, 2025
Published Date: April 8, 2025

A Spectrum of Cardiac Health Risk Assessment Intelligent System

Pankaj Srivastava[1] and Krishna Nandan Kumar[2*]

[1,2] *Department of Mathematics*, *Motilal Nehru National Institute of Technology Allahabad*, *Prayagraj*, 211004, *India*

Corresponding Author: [*]krishna.2022rma05@mnnit.ac.in

Abstract. *Medical diagnosis, particularly for cardiac conditions, is complex due to clinical variability, subjectivity, and incomplete information, which can lead to delays or errors. This article presents the development of an intelligent system using ECG data to enhance clinical efficiency, reduce diagnostic errors, and support medical decision-making. The system smoothly integrates into clinical workflows, analyzes complex data, and enhances patient outcomes. The Python programming language has been used to develop the code for this model.*

Keywords: Linguistic strings, Utility sets, Fuzzy numbers, Linguistic variables, Degree of match, ECG graphs.

1. Introduction

The inherent complexity of medical diagnosis arises from the impreciseness and vague characteristics of symptoms and medical data. This challenge is particularly evident in the medical sciences, where certainty and complete information can hinder accurate diagnosis and treatment. In medicine, practitioners often face situations where clear-cut scientific models and strict diagnostic guidelines are insufficient to account for the variability in patient presentations. Consequently, medical experts frequently rely on their experience, clinical intuition, and judgment to make decisions, particularly in complex cases where the symptoms do not align perfectly with known medical conditions. Although medical professionals gain valuable knowledge through their experiences, utilizing this vast expertise effectively in every case is challenging, particularly during real-time clinical decision-making. The fast-paced nature of clinical settings often limits the ability to tap into their extensive knowledge base fully, making applying it comprehensively to each unique patient scenario challenging.

The concept of decision-making using fuzzy variables was first introduced by Jain, Ramesh [10]. Later, Bellman, R.E. and Zadeh, L.A. [3] extended this idea by proposing the application of fuzzy tools in medicine. Cho, Seongwon, Ersoy, Okan K., and Lehto, Mark [4] developed an algorithm to compute the degree of match (DM) between the antecedent part of a classification rule and an assertion.

In 1994, L.A. Zadeh [19] proposed the concept of Soft Computing for answers to this problem, with the goal of addressing partial truths, imprecision, and ambiguity in decision-making processes. Soft Computing is intended to be more flexible and adaptive to real-world settings where data is frequently ambiguous or missing, in contrast to traditional computing approaches that depend on accurate and complete data. Fuzzy logic is a crucial feature of Soft Computing and is especially important in medical applications. By combining intuition, approximation reasoning, and subjective evaluations—all of which are frequently crucial in medical practice—fuzzy tools mimic human thinking and decision-making.

Soft Computing techniques have become increasingly popular in recent years for the detection and management of cardiac conditions, especially fuzzy tools, which assist in controlling the degree of ambiguity involved in interpreting test findings, patient-reported data, and clinical symptoms. For example, electrocardiograms (ECGs), which employ skill and flexibility to interpret cardiac rhythms and spot abnormalities, are frequently used in the diagnosis of cardiac diseases. The electrocardiograph (ECG) was invented by Dutch scientist Willem Einthoven [2], who made important discoveries that allowed for accurate measurement of the electrical activity of the heart.

In summary, the development of the electrocardiograph was a cumulative process built on the foundations laid by earlier scientists who explored the relationship between electrical impulses and muscle movement. Einthoven's creation was pivotal in medical history, transforming cardiology and paving the way for the modern understanding of heart health.

In 1790, the Italian scientist Aloysio Luigi Galvani [5,8,9] caused a dead frog’s legs to move through electrical stimulation from a completed circuit connecting dissimilar metals. In 1820, the Danish scientist Hans Christian Oersted [11] observed that changes in electrical current could deflect a needle. This led to the creation of the electric rheoscope, later known as the galvanometer, in tribute to Galvani. In 1842, Matteucci [6] introduced and described the term “action potential” after demonstrating that the nerve of a suitably prepared frog limb, when placed over the muscle of a similarly prepared limb and stimulated, could contract the muscle below it.

Willem Einthoven [1,12] (1860–1927), known as the creator of the electrocardiograph, won a Nobel Prize in 1924 for his contributions to electrocardiography. Today, electrocardiography is essential for evaluating patients presenting with cardiac complaints. It is a crucial, non-invasive, cost-effective tool for assessing arrhythmias and ischemic heart disease.

Willem Einthoven built upon these earlier innovations. He realized that a more sensitive and precise instrument was needed to measure the heart's electrical activity accurately. In 1901, Einthoven introduced the string galvanometer, a susceptible device that allowed for the first accurate recordings of the heart's electrical signals. The results were dramatic: the device could produce clear, reproducible tracings of the heart's electrical activity. Einthoven's invention rapidly transformed cardiology. It provided a non-invasive method to diagnose heart conditions, allowing physicians to understand the electrical behavior of the heart in unprecedented detail. Over time, the electrocardiograph evolved, becoming more compact, reliable, and sophisticated, but the fundamental principles remain unchanged. Today, the ECG is a standard medical diagnostic tool used globally to monitor and diagnose heart conditions.

Several researchers have played critical roles in advancing Soft Computing, particularly in cardiac diagnostics. Among them, Srivastava Pankaj and his colleagues have made notable strides in applying Soft Computing techniques to medical applications. For instance, Srivastava Pankaj and Sharma Neeraja [13] developed a Spectrum of Soft Computing Model for Medical Diagnosis that leverages Soft Computing to identify and predict various cardiac conditions. This approach enhances the accuracy of classifying heart rhythm irregularities by blending clinical expertise with fuzzy algorithms.

In addition, Srivastava Pankaj and Srivastava Amit [14] created a comprehensive fuzzy expert system to assess the risk of coronary heart disease (CHD) in the Indian population. This system evaluates risk factors—such as cholesterol levels, blood pressure, lifestyle habits, and family history—to offer personalized recommendations, guiding patients on whether they can maintain their current lifestyle, need to adopt a modified diet, or require medical intervention through drug therapy. This fuzzy expert system has proven to be a valuable resource for healthcare professionals, allowing them to make more informed decisions by providing a detailed analysis of patient risk profiles.

Soft Computing has also demonstrated potential beyond cardiac diseases, showing promise in diagnosing and managing other critical health conditions. For instance, Srivastava Pankaj, Srivastava Amit, and Sirohi Ritu developed a Soft Computing-based classification system for hepatitis B [15]. This system simplifies the diagnostic process and helps determine the stage of the disease. Likewise, the classification of ECG beats, which signals different phases of cardiac conditions, has been further improved by Srivastava Pankaj and Sharma Neeraja [16,17], contributing to detecting and monitoring cardiac anomalies.

Another significant application of Soft Computing is in diabetes management. Srivastava Pankaj, together with Sharma Neeraja and Singh Richa [18], created a diagnostic system using fuzzy tools to assist in diagnosing diabetes and recommending suitable interventions to help patients regulate their blood sugar levels. Their work highlights the importance of developing intelligent systems that integrate with real-time data, offering personalized health recommendations for better diabetes management.

In collaboration with Rajkrishna Mondal, Pankaj Srivastava [7] developed a Diabetes Diagnostic Intelligent Information System, which enhances healthcare professionals' ability to manage diabetes by providing an intelligent system derived from patient data. This system significantly advances diabetes care, showing the decisive role of Soft Computing in medical diagnosis.

This article aims to design and develop an Intelligent system for assessing the current health status of patients. The proposed system utilizes Soft Computing techniques and ECG data from a standard 12-lead ECG machine.

2. Preliminaries

The following features of fuzzy have been considered for designing the model.

2.1 Definition

(i) *Fuzzy set*

Let U *be a non-empty set known as the universe of discourse or simply domain. A fuzzy set A on U is defined by a membership function* $\mu_A : U \to [0,1]$. *The function* μ_A *represents the membership grade of an element* x *in the fuzzy set* A.

$$\boldsymbol{A} = \{(\boldsymbol{x}, \boldsymbol{\mu_A}(\boldsymbol{x})) : \boldsymbol{x} \in \boldsymbol{U}\}$$

(ii) Intersection of two Fuzzy set

Let A and B be two fuzzy sets in the universe of discourse U, with their respective membership functions μ_A and μ_B. The fuzzy intersection of A and B, denoted as $A \cap B$ or the AND operation, is defined as a new fuzzy set. In this set, the membership grade of any element $x \in U$ is given by:

$$\mu_{A\cap B}(x) = \min\{\mu_A(x), \mu_B(x) : x \in U\}.$$

(iii) Fuzzy Rule

In a fuzzy inference system, a fuzzy rule captures uncertain and imprecise knowledge. It connects a condition, which is formed using AND/OR operations on relevant linguistic variables, to a corresponding conclusion.

(iv) Degree of Match

The degree of match (DM) measures how well the inputs and outputs align. It is calculated by using the membership grades of the input and output values in their respective fuzzy sets.

3. Methodology

a. Algorithm

(i) Initially, imprecise and uncertain facts are organized into r input fuzzy sets X_i where $i = 1, 2, \dots, r$ and n output fuzzy sets B_t (where $t = 1, 2, \dots, n$, based on their corresponding possibilities.

(ii) Partition each fuzzy set into k_i distinct linguistic terms, L_{ij}, where $i = 1, 2, \dots, r$ and $j = 1,2, \dots, k_i$.

(iii) Generate $m = k_1 k_2 \dots k_r$ linguistic strings J_K, where $K = 1, 2, \dots, m$, by applying appropriate AND/OR operations to the linguistic terms L_{ij} from each fuzzy set X_i, for $i = 1, 2, \dots, r$ and $j = 1,2, \dots, k_i$.

(iv) Construct an appropriate membership function for each linguistic term in every fuzzy set, based on the available data.

(v) Developed possible fuzzy rules with the help of medical experts.

(vi) Construct of utility matrix U of order $p \times q$. Where p is a number of outputs and q is a number of linguistic variables based on designed fuzzy rules.

(vii) Develop q utility sets, U_I, where $I = 1, 2, 3, \dots, q$, each corresponding to a different alternatives, by applying the operation $x \oplus y = x + y - xy$ for each pair of values $x, y \in U$.

(viii) Construct q maximizing sets U_{MI}, where $I = 1, 2, 3, \dots, q$, corresponding to each alternatives.

(ix) Let U_{OI}, where $I = 1, 2, 3, \dots, q$, represent the set of q optimal fuzzy utility sets. Each U_{OI} is obtained from fuzzy intersection ($\wedge$) of the fuzzy utility set U_I and the maximizing set U_{MI}. The membership function for U_{OI} is given by:

$$\mu_{U_{OI}}(x) = \min\{\mu_{U_I}(x), \mu_{U_{MT}}(x)\}, \qquad \text{for all } x \in X,$$

(x) Select the highest membership value from each optimal utility fuzzy set.

(xi) The best alternative, denoted as B_O , is selected by finding the highest membership value among all available options. It is mathematically written as:

$$B_O = \{\max(\mu_{OI}(x), B_I) : \forall\, I \in U_{OI}\}, \quad where\ I = 1,2,3, \dots \dots ., n$$

(xii) To assess how closely the given inputs, outputs, and computed outputs align with the expected results, the degree of match method is applied to determine the level of satisfaction.

(xiii) The degree of match DM_i for each input $i = 1, 2, 3, \dots, r$ measures how well a precise input value (x_i) aligns with its corresponding fuzzy input set X_i . It is computed by this formula:

$$DM_i = 2\mu_{X_i}(x_i) - 1$$

(xiv) The total degree of match DM_I for the input is calculated by taking the minimum value among all individual degrees of match DM_i for $i = 1, 2, \dots, r$. This can be expressed as:

$$DM_I = \min\{DM_1, DM_2, \dots, DM_r\}$$

and, the degree of match DM_O for the optimal alternatives.

(xv) To assess satisfaction, calculate the difference ($D = |DM_I - DM_O|$). If $0 \le D < 1$ or D is close to zero, it means the output is satisfactorily aligned with the fuzzy inputs.

b. Flow chart

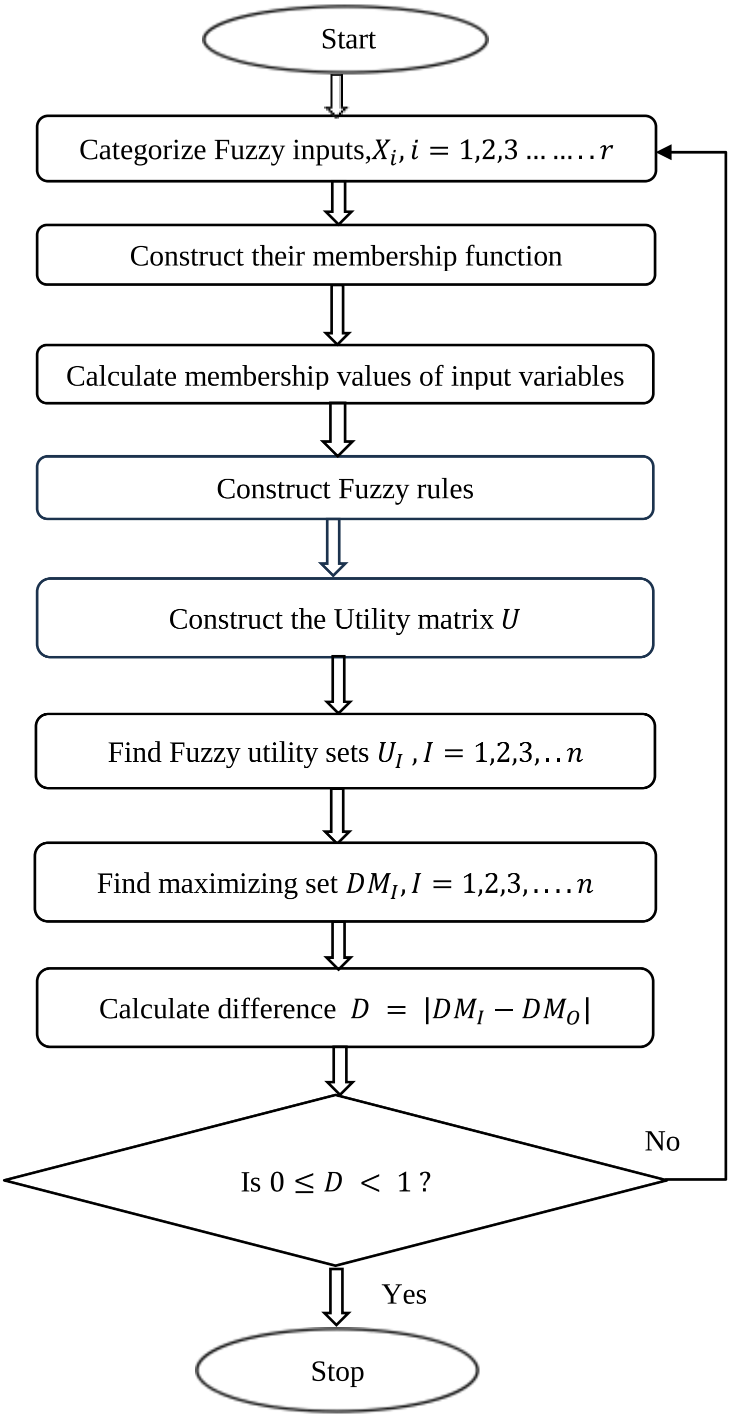

Fig. 1. Flow chart

4. Decision Making Methods

In order to design and develop Intelligent system, we have taken some basic features of ECG graphs as input variables, like Heart rate, QRS complex, RR and PR interval, and we have used trapezoidal and gaussian membership functions for their classification, which are as follows:

a. Heart rate

Heart rate is categorized into 7 linguistic variables, and their membership functions are given below:

Table 1. Heart rate classification

Linguistic variables	Heart rate (bpm)	Membership function
Very Slow	10-45	$\mu_{Very\ slow}(x) = max\left(min\left(\frac{x-10}{10}, 1, \frac{45-x}{15}\right), 0\right)$
Slow	35-60	$\mu_{Slow}(x) = max\left(min\left(\frac{x-35}{7}, 1, \frac{60-x}{10}\right), 0\right)$
Medium	55-70	$\mu_{Medium}(x) = max\left(min\left(\frac{x-55}{5}, 1, \frac{70-x}{5}\right), 0\right)$
Normal	65-100	$\mu_{Normal}(x) = max\left(min\left(\frac{x-65}{10}, 1, \frac{100-x}{15}\right), 0\right)$
Little bit High	90-132	$\mu_{Little\ bit\ high}(x) = max\left(min\left(\frac{x-90}{15}, 1, \frac{132-x}{12}\right), 0\right)$
High	125-150	$\mu_{High}(x) = max\left(min\left(\frac{x-125}{10}, 1, \frac{140-x}{18}\right), 0\right)$
Very High	130-175	$\mu_{Very\ high}(x) = max\left(min\left(\frac{x-130}{30}, 1\right), 0\right)$

b. QRS complex classification

QRS complex is categorized into 4 linguistic variables, and their membership functions are given below:

Table 2. QRS Classification

Linguistic Variables	QRS complex (degree)	Membership functions
Left axis deviation	-90 to -30	$\mu_{Left\ axis\ deviation}(x) = gaussmf(25, -60)$
Normal axis	-30 to 90	$\mu_{Normal\ axis}(x) = gaussmf(7,30)$
Right axis deviation	90 to 180	$\mu_{Right\ axis\ deviation}(x) = gaussmf(28,135)$
Extreme axis deviation	-90 to 180	$\mu_{Extreme\ axis\ deviation}(x) = gaussmf(8,45)$

c. RR interval

RR interval is categorized into 5 linguistic variables, and their membership functions are given below:

Table 3. RR interval classification

Linguistic variables	RR interval	Membership functions
Very short	200-500	$\mu_{Very\ short}(x) = max\left(min\left(\frac{x-200}{100}, 1, \frac{500-x}{100}\right), 0\right)$
Short	480-600	$\mu_{Short}(x) = max\left(min\left(\frac{x-480}{30}, 1, \frac{600-x}{60}\right), 0\right)$
Normal	580-1200	$\mu_{Normal}(x) = max\left(min\left(\frac{x-580}{120}, 1, \frac{1200-x}{300}\right), 0\right)$
Large	1180-1500	$\mu_{Large}(x) = max\left(min\left(\frac{x-1180}{100}, 1, \frac{1500-x}{110}\right), 0\right)$
Very large	1480-1580	$\mu_{Very\ large}(x) = max\left(min\left(\frac{x-1480}{200}, 1\right), 0\right)$

d. PR interval

PR interval is categorized into 5 linguistic variables, and their membership functions are given below:

Table 4. PR interval classification

Linguistic variables	PR interval	Membership function
Very short	20-100	$\mu_{Very\ short}(x) = max\left(min\left(\frac{x-20}{25}, 1, \frac{100-x}{30}\right), 0\right)$
Short	80-121	$\mu_{Short}(x) = max\left(min\left(\frac{x-80}{10}, 1, \frac{121-x}{5}\right), 0\right)$
Normal	100-200	$\mu_{Normal}(x) = max\left(min\left(\frac{x-100}{45}, 1, \frac{200-x}{30}\right), 0\right)$
Large	180-220	$\mu_{Large}(x) = max\left(min\left(\frac{x-180}{10}, 1, \frac{220-x}{15}\right), 0\right)$
Very large	200-320	$\mu_{Very\ large}(x) = max\left(min\left(\frac{x-200}{120}, 1\right), 0\right)$

5. Fuzzy Rule Base

We have developed 700 fuzzy rules based on the suggestions of cardiac experts. However, from the above rules, we have selected the most relevant ones, which are given below.

J_1= If heart rate is "Very Slow," QRS complex is "Left axis deviation," RR interval is "Very Short," and PR interval is "Very Short," then Risk is "Moderate."

J_2= If heart rate is "Very Slow," QRS complex is "Left axis deviation," RR interval is "Very Short," and PR interval is "Short," then Risk is "Moderate."

J_3 = If heart rate is "Very Slow," QRS complex is "Left axis deviation," RR interval is "Very Short," and PR interval is "Normal," then Risk is "High."

J_4= If heart rate is "Very Slow," QRS complex is "Left axis deviation," RR interval is "Very Short," and PR interval is "Large," then Risk is "Very High."

⋮

⋮

J_{313} = If heart rate is "Normal," QRS complex is "Left axis deviation," RR interval is "Normal," and PR interval is "Normal," then Risk is "Normal."

J_{314} = If heart rate is "Normal," QRS complex is "Left axis deviation," RR interval is "Normal," and PR interval is "Large," then Risk is "Moderate."

J_{413} = If heart rate is "Little bit high," QRS complex is "Left axis deviation," RR interval is "Normal," and PR interval is "Normal," then Risk is "Moderate."

J_{414}= If heart rate is "Little bit high," QRS complex is "Left axis deviation," RR interval is "Normal," and PR interval is "Large," then Risk is "High."

⋮

⋮

J_{452} = If heart rate is "Little bit high," QRS complex is "Right axis deviation," RR interval is "Very Short," and PR interval is "Short," then Risk is "High."

J_{453} = If heart rate is "Little bit high," QRS complex is "Right axis deviation," RR interval is "Very Short," and PR interval is "Normal," then Risk is "Very High."

J_{552} = If heart rate is "High," QRS complex is "Right axis deviation," RR interval is "Very Short," and PR interval is "Short," then Risk is "Very High."

J_{553} = If heart rate is "High," QRS complex is "Right axis deviation," RR interval is "Very Short," and PR interval is "Normal," then Risk is "Very High."

⋮

⋮

J_{695} = If Heart rate is "Very High", QRS complex is "Extreme axis deviation," RR interval is "Large," and PR interval is "Large," then Risk is "High."

J_{696} = If heart rate is "Very High," QRS complex is "Extreme axis deviation," RR interval is "Very Large," and PR interval is "Very Short," then Risk is "Very High."

J_{697} = If heart rate is "Very High," QRS complex is "Extreme axis deviation," RR interval is "Very Large," and PR interval is "Short," then Risk is "Very High."

J_{698} = heart rate is "Very High," QRS complex is "Extreme axis deviation," RR interval is "Very Large," and PR interval is "Normal," then Risk is "Moderate."

J_{699} = If heart rate is "Very High," QRS complex is "Extreme axis deviation," RR interval is "Very Large," and PR interval is "Large," then Risk is "High."

J_{700} = If Heart rate is "Very High," QRS complex is "Extreme axis deviation," RR interval is "Very Large," and PR interval is "Large," then Risk is "Very High."

e. Linguistic strings

In accordance with the respective input variables Heart Rate, QRS Complex, RR Interval, and PR Interval there are 700 linguistic strings were generated based on the number of layers for each variable. These strings are as follows:

$$J_1 = \mu_{Heart\ rate(Very\ slow)} \times \mu_{QRS\ complex(Left\ axis\ deviation)} \times \mu_{RR\ interval(Very\ short)} \times \mu_{PR\ interval(Very\ short)}$$

$$J_2 = \mu_{Heart\ rate(Very\ slow)} \times \mu_{QRS\ complex(Left\ axis\ deviation)} \times \mu_{RR\ interval(Very\ short)} \times \mu_{PR\ interval(Short)}$$

$\vdots$

$\vdots$

$$J_{313} = \mu_{Heart\ rate(Normal)} \times \mu_{QRS\ complex(Left\ axis\ deviation)} \times \mu_{RR\ interval(Normal)} \times \mu_{PR\ interval(Normal)}$$

$$\mathrm{J}_{314} = \mu_{\text{Heart rate(Normal)}} \times \mu_{\text{QRS complex(Left axis deviation)}} \times \mu_{RR\ interval(Normal)} \times \mu_{PR\ interval(Large)}$$

$$J_{413} = \mu_{Heart\ rate(Little\ bit\ high)} \times \mu_{QRS\ complex(Left\ axis\ deviation)} \times \mu_{RR\ interval(Normal)} \times \mu_{PR\ interval(Normal)}$$

$$J_{414} = \mu_{Heart\ rate(Little\ bit\ high)} \times \mu_{QRS\ complex(Left\ axis\ deviation)} \times \mu_{RR\ interval(Normal)} \times \mu_{PR\ interval(Large)}$$

$\vdots$

$\vdots$

$$J_{452} = \mu_{Heart\ rate(Little\ bit\ high)} \times \mu_{QRS\ complex(Right\ axis\ deviation)} \times \mu_{RR\ interval(Very\ short)} \times \mu_{PR\ interval(Short)}$$

$$J_{453} = \mu_{Heart\ rate(Little\ bit\ high)} \times \mu_{QRS\ complex(Right\ axis\ deviation)} \times \mu_{RR\ interval(Very\ short)} \times \mu_{PR\sim interval(normal)}$$

$$J_{552} = \mu_{Heartrate(High)} \times \mu_{QRS\ complex(Right\ axis\ deviation)} \times \mu_{RR\ interval(Very\ short)} \times \mu_{PR\ interval(Short)}$$

$$J_{553} = \mu_{Heart\ rate(High)} \times \mu_{QRS\ complex(Right\ axis\ deviation)} \times \mu_{RR\ interval(Very\ short)} \times \mu_{PR\ interval(normal)}$$

$\vdots$

$\vdots$

$$J_{698} = \mu_{Heart\ rate(Very\ high)} \times \mu_{QRS\ complex(Extreme\ axis\ deviation)} \times \mu_{RR\ interval(Very\ large)} \times \mu_{PR\ interval(Normal)}$$

$$J_{699} = \mu_{Heart\ rate(Very\ high)} \times \mu_{QRS\ complex(Extreme\ axis\ deviation)} \times \mu_{RR\ interval(Very\ large)} \times \mu_{PR\ interval(Large)}$$

$$J_{700} = \mu_{Heart\ rate(Very\ high)} \times \mu_{QRS\ complex(Extreme\ axis\ deviation)} \times \mu_{RR\ interval(Very\ large)} \times \mu_{PR\ interval(Large)}$$

f. Output classification

The status of heart health is categorized into 5 outputs:

O_1= Low, O_2=Normal, O_3=Moderate, O_4=High, O_5= Very high.

6. Computation

The utility matrix U designed of order 5×700 as per fuzzy rule base:

$$U = \begin{pmatrix} 40 & 12 & \dots & 18 & 10 & \dots & 15 & 12 \\ 50 & 50 & \dots & 42 & 20 & \dots & 45 & 25 \\ 35 & 35 & \dots & 60 & 65 & \dots & 75 & 60 \\ 45 & 45 & \dots & 33 & 50 & \dots & 65 & 55 \\ 55 & 55 & \dots & 71 & 35 & \dots & 55 & 40 \end{pmatrix}$$

Case-I

Heart rate=131 bpm, QRS complex=90°, RR interval= 458 ms, PR interval=112 ms

The given fuzzy set which represents the state of concerned patients:

Heart rate={(Very slow,0),(Slow,0),(Medium,0),(Normal,0.46666667),(Little bit high,0.2),(High,0), (Very high,0)}

QRS complex={(Left axis deviation,0.910909),(Normal axis,0),(Right axis deviation,0),

(Extreme axis deviation, 0)}

RR interval={(Very short,0),(Short,0),(Normal,0.5416667),(Large,0),(very large,0)}

PR interval={(Very short,0),(Short,0),(Normal,0.433333),(Large,0.7),(very large,0)}

The state of the system of concerned patients is as follows:

$A = (0.09977811, J_{313}), (0.16118015, J_{314}), (0.04276211, J_{413}), (0.06907730, J_{414})$

The fuzzy utilities with each alternatives sets are as follows:

$U_1 = \{(0.00962048,20), (0.00256546,10), (0.08081202,15), (0.02154987,12)\}$

$U_2 = \{(0.00962048,35), (0.00256546,20), (0.08081202,45), (0.02154987,25)\}$

$U_3 = \{(0.00962048,80), (0.00256546,65), (0.08081202,75), (0.02154987,60)\}$

$U_4 = \{(0.08965505,65), (0.00256546,50), (0.02154987,55)\}$

$U_5 = \{(0.00962048,50), (0.00256546,35), (0.08081202,55), (0.02154987,40)\}$

The maximizing sets corresponding to each alternatives are as follows:

$U_{M1} = \{(0.00024414,20), (0.00000381,10), (0.00004345,15), (0.00001139,12)\}$

$U_{M2} = \{(0.00701243,35), (0.0024414,20), (0.03167635,45), (0.00093132,25)\}$

$U_{M3} = \{(1.0000000,80), (0.28770024,65), (0.67893416,75), (0.17797852,60)\}$

$U_{M4} = \{(0.28770024,65), (0.05960464,50), (0.10559326,55)\}$

$U_{M5} = \{(0.05960464,50), (0.00701243,35), (0.10559326,55), (0.01562500,40)\}$

The optimal fuzzy utilities sets are as follows:

$U_{01} = \{(0.00024414,20), (0.00000381,10), (0.00004345,15), (0.00001139,12)\}$

$U_{02} = \{(0.00701243,35), (0.00024414,20), (0.03167635,45), (0.00093132,12)\}$

$U_{03} = \{(0.00962048,80), (0.00256546,20), (0.08081202,45), (0.02154987,60)\}$

$U_{04} = \{(0.08965505,65), (0.00256546,50), (0.02154987,55)\}$

$U_{05} = \{(0.00962048,50), (0.00256546,35), (0.08081202,55), (0.02154987,40)\}$

The set of optimal alternatives are as follows:

B_0={ (0.00024414, Low), (0.03167635, Normal), (0.08081202, Moderate), (0.08965505, High), (0.08081202, Very high)}

The sets having the greatest grade of membership value, hence the best alternative, is High.

Fig. 2. Output for case-I

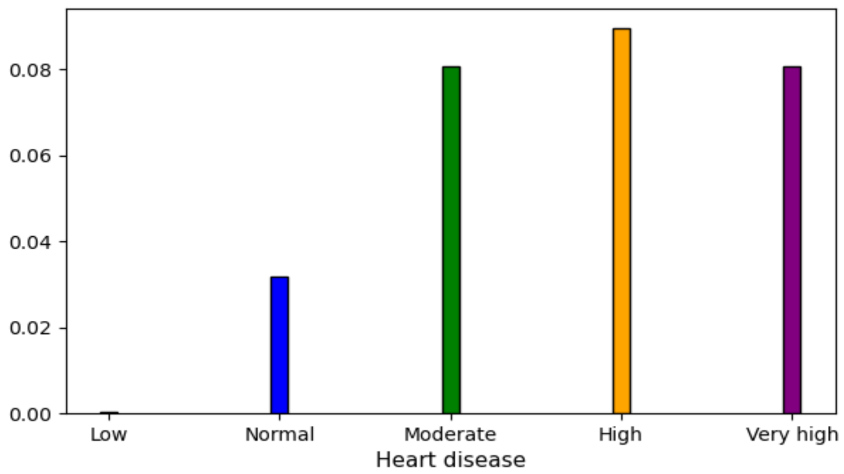

The above graphical sketches clearly indicate that the patients are in the high-risk category.
Degree of match for inputs as given below:

$DM_{I1'} = 2\mu_{Heart\ rate_{Little\ bit\ high}}(131) = 2(0.08333333) - 1 = -0.83333334$

$DM_{I1''} = 2\mu_{Heart\ rate_{High}}(131) = 2(0.7) - 1 = 0.40000000$

$DM_{I2} = 2\mu_{QRS\ complex_{Right\ axis\ deviation}}(90°) = 2(0.2748708) - 1 = -0.4502584$

$DM_{I3} = 2\mu_{RR\ interval_{Very\ short}}(458) = 2(0.42) - 1 = -0.16$

$DM_{I4'} = 2\mu_{PR\ interval_{Short}}(112) = 2(1) - 1 = 1.00000000$

$DM_{I4''} = 2\mu_{PR\ interval_{Normal}}(112) = 2(0.26666667) - 1 = -0.4666666$

To verify the consistency between input and output observations, the degree of match for the input (DM_I) is determined the minimum value among the given inputs:

$$DM_I = \min\{-0.83333334, 0.4, -0.4502584, -0.16, 1, -0.4666666\} = -0.83333334.$$

The degree of match for the optimal alternative (DM_0) is calculated using the given formula:

$$DM_0 = 2(0.08965505) - 1 = -0.8206899.$$

The absolute difference between the two degrees of match is computed as:

$$D = |DM_I - DM_0| = |-0.83333334 - (-0.8206899)| = 0.01264344.$$

This difference within the range ([0,1]) and is very close to zero, indicating that the noise between the input and output observations are close to each other. This minimal difference confirms a high level of satisfaction.

Case-II

Heart rate = 93 bpm; QRS complex= $-49.2°$; RR interval = 645 ms; PR interval=187 ms

The fuzzy sets represents the state of concerned patient:

Heart rate = {(Very short,0),(Short,0),(Medium,0),(Normal,0.46666667),(Little bit high,0.2),(High,0),(Very high,0)}

QRS complex={(Left axis deviation,0.910909),(Normal axis,0),(Right axis deviation,0),(Extreme axis deviation,0)}

RR interval={(Very short,0),(Short,0),(Normal,0.5416667),(Large,0),(Very large,0)}

PR interval={(Very short,0),(Short,0),(Normal,0.43333333),(Large,0.7),(Very large,0)}

The state of the system of concerned patients is as follows:

$A = \{(0.09977811, J_{313}), (0.16118015, J_{314}), (0.04276211, J_{413}), (0.06907730, J_{414})\}$

The fuzzy utility values associated with each set of alternatives are as follows:

$U_1 = \{(0.09977811,40), (0.16118015,12), (0.0427621,18), (0.06907730,24)\}$

$U_2 = \{(0.09977811,50), (0.16118015,38), (0.0427621,42), (0.06907730,29)\}$

$U_3 = \{(0.09977811,35), (0.16118015,55), (0.0427621,60), (0.06907730,34)\}$

$U_4 = \{(0.09977811,45), (0.16118015,48), (0.0427621,33), (0.06907730,28)\}$

$U_5 = \{(0.09977811,55), (0.16118015,25), (0.0427621,71), (0.06907730,24)\}$

The maximizing sets corresponding to each alternative are presented as follows:

$U_{1M} = \{(0.0567553,40), (0.00013792,12), (0.00104730,18), (0.00441331,24)\}$

$U_{2M} = \{(0.17320414,50), (0.02169092,38), (0.07243604,42), (0.01136837,29)\}$

$U_{3M} = \{(0.02911042,35), (0.27894699,55), (0.07243604,60), (0.01136837,34)\}$

$U_{4M} = \{(0.10227531,45), (0.14122592,48), (0.02169092,33), (0.00953890,28)\}$

$U_{5M} = \{(0.27898300,55), (0.14121548,25), (0.02169092,71), (0.00953890,24)\}$

The optimal fuzzy utility sets are given as follows:

$U_{01} = \{(0.05675553,40), (0.0013792,12), (0.00104730,18), (0.00441331,24)\}$

$U_{02} = \{(0.09977811,40), (0.02169092,38), (0.0427621,42), (0.01136837,29)\}$

$U_{03} = \{(0.02911042,35), (0.16118015,55), (0.0427621,60), (0.01136837,34)\}$

$U_{04} = \{(0.09977811,45), (0.14122592,48), (0.021690927,71), (0.00953890,24)\}$

The set of optimal alternative are as follows:

B_o={(0.05675553, Low), (0.09977811, Normal), (0.16118015, Moderate), (0.14122592, High), (0.14121548, Very high)}

The sets having the greatest grade of membership value, hence the best alternative, is Moderate.

Fig.3. Output for case-II

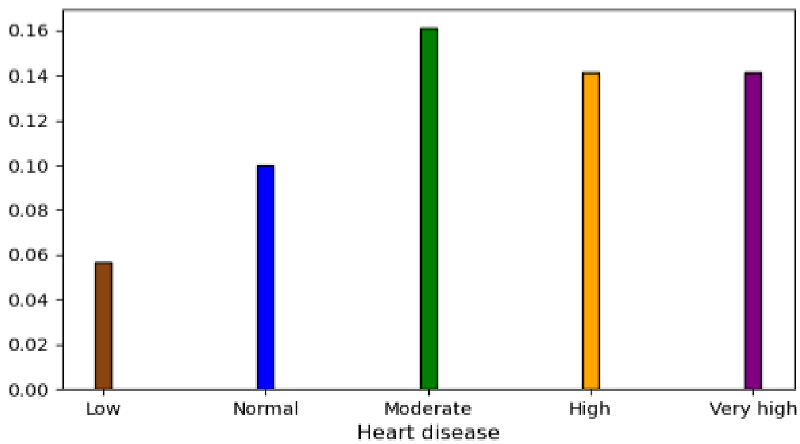

The above graphical sketches clearly indicate that the patients are in the moderate-risk category.

Degree of match for input variables are as follows:

$$DM_{I1'} = 2\mu_{Heart\ rate_{Little\ bit\ high}}(93) = 2(0.46666666) - 1 = -0.06666668$$

$$DM_{I1''} = 2\mu_{Heart\ rate_{High}}(93) = 2(0.2) - 1 = -0.600$$

$$DM_{I2} = 2\mu_{QRS\ complex_{Left\ axis\ deviation}}(-49.2°) = 2(0.910909) - 1 = 0.8218185$$

$$DM_{I3} = 2\mu_{RR\ interval_{Normal}}(645) = 2(0.5416666) - 1 = 0.0833332$$

$$DM_{I4'} = 2\mu_{PR\ interval_{Normal}}(187) = 2(0.43333333) - 1 = -0.13333334$$

$$DM_{I4''} = 2\mu_{PR\ interval_{Large}}(187) = 2(0.7) - 1 = 0.4$$

The degree of match for the input (DM_I) is calculated the minimum value among the given inputs:

$DM_I = \min\{-0.06666668, -0.6, 0.8218185, 0.08333332, -0.13333334, 0.4, -0.13333334, -0.13333334\} = -0.6.$

The degree of match for the optimal alternative (DM_0) is determined using the formula:

$$DM_0 = 2(0.16118015) - 1 = -0.6776397.$$

The difference between (D_{MI}) and (D_{M0}) is computed as:

$$D = |DM_I - DM_0| = |-0.6 - (-0.6776397)| = 0.0776397.$$

This difference lies within the range ([0,1]) and is close to zero. This indicates that the noise between the input and output observations is close to each other, verifying a high level of satisfaction. Similarly, we have computed the remaining patient’s data.

7. Conclusion

This research paper shows that a Soft Computing diagnostic system can effectively replicate expert thinking, making it useful for handling complex cases. The proposed method will help in designing and developing a Soft Computing-based risk assessment system to support medical experts in classifying the severity of cardiac issues.

Conflict of Interest Declaration

The authors affirm that they have no financial interests, personal relationships, or other affiliations that could have influenced the research and findings presented in this paper.

Acknowledgments

I sincerely thank Dr. R.P. Singh (Prabha Clinic, Phaphamau, Prayagraj) and Dr. Pankaj Singh (Cardiologist, Shardha Hospital, Jaunpur) for their invaluable guidance and insightful contributions. Their expertise and thoughtful recommendations have greatly enhanced the clarity and impact of this work. I deeply appreciate their generosity in sharing their knowledge and their dedication to advancing medical science.

References

[1] AlGhatrif, M., & Lindsay, J. **(2012)**. A brief review: history to understand fundamentals of electrocardiography. *Journal of community hospital internal medicine perspectives*, **2(1)**: 14383.

[2] Barold, S. S. **(2003)**. Willem Einthoven and the birth of clinical electrocardiography a hundred years ago. *Cardiac electrophysiology review*, **7**: 99-104.

[3] Bellman, R. E., & Zadeh, L. A. **(1970)**. Decision-making in a fuzzy environment. *Management science*, **17(4)**: B-141.

[4] Cho, S., Ersoy, O. K., & Lehto, M. **(1992)**. An algorithm to compute the degree of match in fuzzy systems. *Fuzzy Sets and Systems*, **49(3)**: 285-299.

[5] Galvani, L. (1791). De viribus electricitatis in motu musculari. Commentarius. *De Bonoiensi Scientiarum et Artium Intituo atque Academie Commentarii*, **7**: 363-418.

[6] Guyton, A. C., & Hall, J. E. **(2011)**. *Guyton and Hall textbook of medical physiology*. Elsevier.

[7] Mondal, R., & Srivastava, P. **(2021)**. Design and Development of an Intelligent System to Assess Kidney Performances of Persons Suffering from Diabetes. *International Transaction Journal of Engineering, Management, & Applied Sciences & Technologies*, **12(4)**: 1-7.

[8] Piccolino, M. **(1998)**. Animal electricity and the birth of electrophysiology: the legacy of Luigi Galvani. *Brain research bulletin*, **46(5)**: 381-407.

[9] Piccolino, M. **(2006)**. Luigi Galvani's path to animal electricity. *Comptes rendus biologies*, **329(5-6)**: 303-318.

[10] Ramesh, J. **(1976)**. Decision making in the Presence of Fuzzy Variables.

[11] Rivera-Ruiz, M., Cajavilca, C., & Varon, J. **(2008)**. Einthoven's string galvanometer: the first electrocardiograph. *Texas Heart Institute Journal*, **35(2)**: 174.

[12] Snellen, H. A. **(1994)**. *Willem Einthoven (*1860–1927*) Father of electrocardiography: Life and work, ancestors and contemporaries*. Springer Science & Business Media.

[13] Srivastava, P., & Sharma, N. **(2014)**. A spectrum of soft computing model for medical diagnosis. *Applied Mathematics & Information Sciences*, **8(3)**: 1225.

[14] Srivastava, P., Srivastava, A., Burande, A., & Khandelwal, A. **(2013)**. A note on hypertension classification scheme and soft computing decision making system. *International Scholarly Research Notices*, **2013(1)**: 342970.

[15] Srivastava, P., Srivastava, A., & Sirohi, R. **(2012)**. Soft computing tools and classification criterion for Hepatitis B. *International Journal of Research and Reviews in Soft & Intelligent Computing*, **2(2)**: 147-153.

[16] Srivastava, P., & Sharma, N. **(2021)**. Intelligent System for ECG Beat Classification. In *Mathematical, Computational Intelligence and Engineering Approaches for Tourism, Agriculture and Healthcare* (pp. 121-132). Singapore: Springer Singapore.

[17] Srivastava, P., & Sharma, N. **(2019)**. Fuzzy risk assessment information system for coronary heart disease. *International Conference on Innovative Computing and Communications: Proceedings of ICICC* 2018, **2**: 159-170. Springer Singapore.

[18] Srivastava, P., Sharma, N., & Singh, R. **(2012)**. Soft computing diagnostic system for diabetes. *International Journal of Computer Applications*, **47**(18):22-27.

[19] Zadeh, L. A. **(1994)**. Soft computing and fuzzy logic. *IEEE software*, **11(6)**: 48-56.

Nepal Journal of Mathematical Sciences (NJMS)
ISSN: 2738-9928 (online), 2738-9812 (print)
Vol. 6, No. 1, 2025 (February): 35-44
DOI: 10.3126/njmathsci.v6i1.77374
©School of Mathematical Sciences,
Tribhuvan University, Kathmandu, Nepal

Research Article
Received Date: January 3, 2025
Accepted Date: March 25, 2025
Published Date: April 8, 2025

On Some Sequence Spaces of Bi-complex Numbers

Purushottam Parajuli[1*], Narayan Prasad Pahari[2], Jhavi Lal Ghimire[2] & Molhu Prasad Jaiswal[3]

[1]*Department of Mathematics, Tribhuvan University, Prithvi Narayan Campus Pokhara, Nepal*
[2] *Central Department of Mathematics, Tribhuvan University, Kirtipur, Kathmandu, Nepal*
[3] *Department of Mathematics, Tribhuvan University, Bhairahawa Campus, Bhairahawa, Nepal*

Corresponding Author: [*]pparajuli2017@gmail.com

Abstract: *In 1892, Segre introduced the concept of bi-complex numbers. The main contribution in bi-complex analysis was the pioneering works in Functional analysis. It is a new subject, not only relevant from a mathematical point of view, but also has significant applications in physics and engineering.*

This article provides an overview of bi-complex numbers and examines the completeness of certain sequence spaces of bi-complex numbers. Additionally, the study explores their algebraic, topological, and geometric properties, contributing to a deeper understanding of these spaces.

Keywords: Bi-complex numbers, Euclidean norm, Banach space, Convexity, Uniform convexity

1. Introduction

Bi-complex numbers have been studied for quite a long time, and a lot of work has been done in this area. In 1892, Segre [18] introduced the concept of bi-complex numbers. The most comprehensive study of bi-complex numbers was done by Price [15]. Alpay et al. [1] developed a general theory of functional analysis with bi-complex scalars. In 2004, Rochon and Shapiro [16] studied some algebraic properties of Bi-complex and hyperbolic numbers. Later, Wagh [21], Degirmen and Sağır [6], Bera and Tripathy [3, 4], Sager and Sağır [17], and many researchers have studied the algebraic, topological, and geometric properties of bi-complex sequence spaces.

Definition 1.1. [17] A bi-complex number is denoted by γ and defined as,

$$\begin{aligned}\gamma &= x_1 + i_1x_2 + i_2x_3 + i_1i_2x_4\\ &= (x_1 + i_1x_2) + i_2(x_3 + i_1x_4)\\ &= z_1 + i_2 z_2, \text{ where, } x_1, x_2, x_3, x_4 \in \mathbb{C}_0,\ z_1, z_2 \in \mathbb{C}_1,\end{aligned}$$

$i_1^2 = i_2^2 = -1$, $i_1 i_2 = i_2 i_1$ and $\mathbb{C}_0$, $\mathbb{C}_1$, are the set of real and complex numbers respectively, $i_1 i_2$ is a hyperbolic unit whose square is 1.

The set of bi-complex numbers is denoted by $\mathbb{C}_2$ and is defined by

$$\mathbb{C}_2 = \{z_1 + i_2 z_2 : z_1, z_2 \in \mathbb{C}_1\}$$

There are three types of conjugations on bi-complex numbers (Rochan and Shapiro [16])

i) i_1 - conjugation of $\gamma = z_1 + i_2 z_2$ is $\gamma^* = \overline{z_1} + i_2\overline{z_2}$

ii) i_2 - conjugation of γ is $\bar{\gamma} = z_1 - i_2 z_2$

iii) $i_1 i_2$ - conjugation of γ is $\gamma' = \overline{z_1} - i_2\,\overline{z_2}$

Definition 1.2. A bi-complex number $\gamma = z_1 + i_2 z_2$ is hyperbolic if $\gamma' = \gamma$ $or\ Im(z_1) = Re(z_2) = 0$. The set of all hyperbolic numbers is denoted by H and is defined by $H = \{x_1 + i_1 i_2 x_2 : x_1, x_2, \in \mathbb{C}_0\}$

For example, $\gamma = 1 + 2\, i_1 i_2$ is a hyperbolic number.

The bi-complex number $\gamma = z_1 + i_2 z_2$ is singular if $|z_1^2 + z_2^2| = 0$ and non-singular if $|z_1^2 + z_2^2| \neq 0$.

In $\mathbb{C}_2$, there are exactly two non-trivial idempotent elements e_1 and e_2 defined by

$$e_1 = \frac{1 + i_1 i_2}{2} \text{ and } e_2 = \frac{1 - i_1 i_2}{2}$$

Obviously, $e_1 + e_2 = 1$, $e_1 e_2 = e_2 e_1 = 0$, $e_1^2 = e_1$ and $e_2^2 = e_2$

Every bi-complex number $\gamma = z_1 + i_2 z_2$ had unique idempotent representation as $\gamma = \mu_1 e_1 + \mu_2 e_2$, where $\mu_1 = z_1 - i_1 z_2$ and $\mu_2 = z_1 + i_1 z_2$ are the idempotent components of γ . The set $\{e_1, e_2\}$ forms an idempotent basis of $\mathbb{C}_2$. Equipped with co-ordinate wise addition, real scalar multiplication and term by term multiplication, $\mathbb{C}_2$ becomes a commutative ring with unity.

Algebraic structures of $\mathbb{C}_2$ differ from that of $\mathbb{C}_1$ in many aspects. A few of them are mentioned below.

(i) Non-invertible elements exist in $\mathbb{C}_2$

(ii) Non-invertible idempotent elements exist in $\mathbb{C}_2$

(iii) Non-trivial zero divisors exist in $\mathbb{C}_2$

The norm (Euclidean norm) on $\mathbb{C}_2$ is defined by

$$\|\gamma\|_{C_2} = \sqrt{x_1^2 + x_2^2 + x_3^2 + x_4^2} = \sqrt{|z_1|^2 + |z_2|^2} = \sqrt{\frac{|\mu_1|^2 + |\mu_2|^2}{2}}.$$

Definition 1.3. A sequence in $\mathbb{C}_2$ is a function defined by $\gamma : \mathbb{N} \to \mathbb{C}_2$, $\gamma = (\gamma_k)$, where $\gamma_k \in \mathbb{C}_2$.

The sequence (γ_k) of bi-complex numbers is said to be convergent to $\gamma \in \mathbb{C}_2$ iff for each $\varepsilon > 0$ there corresponds an $n(\varepsilon) \in \mathbb{N}$ such that

$$\|\gamma_k - \gamma\|_{\mathbb{C}_2} < \varepsilon, \text{ for all } k \geq n(\varepsilon). \text{ It is written as } \lim_{k\to\infty} \gamma_k = \gamma.$$

The sequence (γ_k) of bi-complex numbers is said to be a Cauchy sequence if for every $\varepsilon > 0$ there exists a positive integer $n(\varepsilon) \in \mathbb{N}$ such that

$$\|\gamma_m - \gamma_n\|_{\mathbb{C}_2} < \varepsilon, \text{ for all } m, n \geq n(\varepsilon).$$

Definition 1.4. Let E be a sequence space of bi-complex numbers and $\breve{E} = \{(u_n) \in \omega(\mathbb{C}_2)$, there exists $x_n \in$ E such that $\|u_n\|_{\mathbb{C}_2} \leq \|x_n\|_{\mathbb{C}_2}$ for all $n \in \mathbb{N}$. Then E is said to be solid or normal if $\breve{E} \subset E$.

Definition 1.5. A sequence space E of bi-complex numbers is said to be symmetric if $(\gamma_k) \in$ E implies $\gamma_{\pi(k)} \in$ E where π is the permutation of $\mathbb{N}$

Definition 1.6.[6] Let E be a subset of linear space X. Then E is said to be convex if $(1-\lambda)\,x + \lambda y \in$ E for all $x, y \in$ E and all scalar $\lambda \in [0\ 1]$.

Definition 1.7.[6] A Banach space X is said to be strictly convex if $x, y \in S_X$ with $x \neq y$ implies that $\|(1-\lambda)\,x + \lambda y\| < 1$ for all $\lambda \in (0\ 1)$.

Definition 1.8.[6] A Banach space X is said to be uniformly convex if, to each $\varepsilon > 0,\ 0 < \varepsilon \le 2$ such that for all $x, y \in S_X$, where S_X represents the unit sphere, there corresponds a $\delta(\varepsilon) > 0$ such that the conditions

$$\| x \| = \| y \| = 1, \| x - y \| \ge \varepsilon \Longrightarrow \frac{1}{2} \| x + y \| \le 1 - \delta(\varepsilon).$$

2. Some sequence spaces over the set of bi-complex numbers.

If ω denotes the set of all functions from the set of positive integers $\mathbb{N}$ to the field $\mathbb{C}$ of complex numbers then it becomes a vector space. Any Sequence space is defined as a set of all sequences $x = (x_n)$ linear subspace of ω over the field $\mathbb{C}$ with the usual operations defined as

$$(x_n) + (y_n) = (x_n + y_n) \text{ and } \lambda(x_n) = (\lambda x_n).$$

Recently, several researchers, including Ghimire & Pahari [8], Pahari [12], Paudel, Pahari & Kumar [13],Pokharel , Pahari, & Paudel [14] and Srivastava & Pahari[19] have studied the theory of vector-valued sequence spaces using Banach sequences.

The notations $\omega(\mathbb{C}_2)$, $l_\infty(\mathbb{C}_2)$, $c(\mathbb{C}_2)$, $c_0(\mathbb{C}_2)$, $l_p(\mathbb{C}_2)$ denote the class of all bounded, convergent, null and absolutely p-summable bi-complex sequences [13].

$$\omega(\mathbb{C}_2) = \{x = (x_k): x_k \in \mathbb{C}_2 \text{ for all } k \in \mathbb{N}\}$$

$$l_\infty(\mathbb{C}_2) = \{x = (x_k): x_k \in \omega(\mathbb{C}_2) : \sup_{k \in \mathbb{N}} || x_k ||_{C_2} < \infty\}$$

$$c(\mathbb{C}_2) = \{x = (x_k): x_k \in \omega(\mathbb{C}_2), \exists\ l \in \mathbb{C}_2: \lim_{k \to \infty} x_k = l\}$$

$$c_0(\mathbb{C}_2) = \{x = (x_k): x_k \in \omega(\mathbb{C}_2): \lim_{k \to \infty} x_k = 0\}$$

$$l_p(\mathbb{C}_2) = \{x = (x_k): x_k \in \omega(\mathbb{C}_2): \sum_{k=1}^{\infty} ||x_k||_{c_2}^p < \infty\}$$

Lemma 2.1.[16] (Bi-complex Minkowski's inequality)

Let p and q be real numbers with $1 < p < \infty$ and $x_k, y_k, \in \mathbb{C}_2$ for $k \in \{1, 2, \ldots, n\}$. Then,

$$\left[\left(\sum_{k=1}^{n} || x_k + y_k ||_{\mathbb{C}_2}^p\right)\right]^{\frac{1}{p}} \le \left[\left(\sum_{k=1}^{n} || x_k ||_{\mathbb{C}_2}^p\right)\right]^{\frac{1}{p}} + [(\sum_{k=1}^{n} || y_k||_{\mathbb{C}_2}^p)^{\frac{1}{p}}\}]$$

Lemma 2.2.[6] Let p be a real number with $0 < p \le 1$, $x = (x_k)$ and $y = (y_k) \in \mathbb{C}_2$.

Then, we have $\| x + y\|_{\mathbb{C}_2}^p \le \|x\|_{\mathbb{C}_2}^p + \|y\|_{\mathbb{C}_2}^p$

Lemma 2.3.[6] Let p be a real number with $2 \le p < \infty$ and $x = (x_k), y = (y_k) \epsilon\, \mathbb{C}_2$. Then, we have

$$\|x + y\|_{\mathbb{C}_2}^p + ||x - y||_{\mathbb{C}_2}^p \le 2^{p-1}(||x||_{\mathbb{C}_2}^p + ||y||_{\mathbb{C}_2}^p||)$$

Several workers Basar [2], Degirmen & Sagir [5], Ellidokuzoglu & Demiriz [7] , Güngör [9] , Hardy [10], Kumar & Tripathy[11], Srivastava & Srivastava [20] have made substantial contributions to the theory of series and bicomplex numbers and sequences.

3.Main Results

In this section, we present some theorems and examples exploring some algebraic and topological properties of the sequences of bi-complex numbers.

Theorem 3.1. The space $l_\infty(\mathbb{C}_2)$ is a bi-complex solid space.

Proof.

Let $(x_n) \in \tilde{l}_\infty(\mathbb{C}_2)$, then there exists a sequence $(y_n) \in l_\infty(\mathbb{C}_2)$ such that

$$|| x_n||_{\mathbb{C}_2} \le || y_n||_{\mathbb{C}_2} \text{ for all } n \in \mathbb{N}.$$

Therefore, sup $\{\|y_n\|_{\mathbb{C}_2} : \mathrm{n} \in \mathbb{N}\} < \infty$ and so, $\sup\{\|x_n\|_{\mathbb{C}_2} : n \in \mathbb{N}\} < \infty$.

This shows that $(x_n) \in l_\infty(\mathbb{C}_2)$. Thus $(x_n) \in \tilde{l}_\infty(\mathbb{C}_2)$ implies $(x_n) \in l_\infty(\mathbb{C}_2)$.

So, $\tilde{l}_\infty(\mathbb{C}_2) \subset l_\infty(\mathbb{C}_2)$. Hence $l_\infty(\mathbb{C}_2)$ is a bi-complex solid space.

Theorem 3. 2. The space $l_\infty(\mathbb{C}_2)$ is a bi-complex symmetric space.

Proof.

Let $(x_n) \in l_\infty(\mathbb{C}_2)$ and $\sigma \in \pi$. Then, $\sigma : \mathbb{N} \to \mathbb{N}$ is a bijective function. So, we have

$$\{\|x_{\sigma(n)}\|_{\mathbb{C}_2} : n \in \mathbb{N}\} = \{\|x_n\|_{\mathbb{C}_2} : n \in \mathbb{N}\}.$$

Also, $\sup\{\|x_{\sigma(n)}\|_{\mathbb{C}_2} : n \in \mathbb{N}\} = \sup\{\|x_n\|_{\mathbb{C}_2} : n \in \mathbb{N}\}$.

Since $(x_n) \in l_\infty(\mathbb{C}_2)$, $sup\{\|x_n\|_{\mathbb{C}_2} : n \in \mathbb{N}\} < \infty$. Also, $\sup\{\|x_{\sigma(n)}\|_{\mathbb{C}_2} : n \in \mathbb{N}\} < \infty$.

This result shows that $(x_{\sigma(n)}) \in l_\infty(\mathbb{C}_2)$. Hence $l_\infty(\mathbb{C}_2)$ is a bicomplex symmetric space.

Theorem 3.3. The space $l_p(\mathbb{C}_2)$ is a bi-complex solid space for $0 < p < \infty$.

Proof.

Let $(x_n) \in \tilde{l}_p(\mathbb{C}_2)$, then there exists a sequence $(y_n) \in l_p(\mathbb{C}_2)$such that

$\|x_n\| \leq \|y_n\|$ for all $n \in \mathbb{N}$.

Also, $\|x_n\|_{\mathbb{C}_2}^p \leq \|y_n\|_{\mathbb{C}_2}^p$for all $n \in \mathbb{N}$.

Since the series $\sum_{n=1}^{\infty} \|y_n\|_{\mathbb{C}_2}^p$ is convergent, the comparison test for convergent series implies that the series $\sum_{n=1}^{\infty} \|x_n\|_{\mathbb{C}_2}$ is also convergent. So, $(x_n) \in l_p(\mathbb{C}_2)$.

Thus $(x_n) \in \tilde{l}_p(\mathbb{C}_2)$ imples $(x_n) \in l_p(\mathbb{C}_2)$. Hence $\tilde{l}_p(\mathbb{C}_2) \subset l_p(\mathbb{C}_2)$.

So, $l_p(\mathbb{C}_2)$ is a bi-complex solid space.

Theorem 3.4. The space $l_p(\mathbb{C}_2)$ is a bi-complex symmetric space for $0 < p < \infty$.

Proof.

Let $(x_n) \in l_p(\mathbb{C}_2)$ and $\sigma \in \pi$. Since $\sigma : \mathbb{N} \to \mathbb{N}$ is a bijective function, we can write

$$\left\{\|x_{\sigma(n)}\|_{\mathbb{C}_2} : n \in \mathbb{N}\right\} = \{\|x_n\|_{\mathbb{C}_2} : n \in \mathbb{N}\}$$

and so, $\left\{\|x_{\sigma(n)}\|_{\mathbb{C}_2}^p : n \in \mathbb{N}\right\} = \left\{\|x_n\|_{\mathbb{C}_2}^p : n \in \mathbb{N}\right\}$ holds.

Then, $\sum_{n=1}^{\infty} \|x_{\sigma(n)}\|_{\mathbb{C}_2}^p = \sum_{n=1}^{\infty} \|x_n\|_{\mathbb{C}_2}^p$

Since, $(x_n) \in l_p(\mathbb{C}_2)$, $\sum_{n=1}^{\infty} \|x_n\|_{\mathbb{C}_2}^p$ converges.

Also, the series $\sum_{n=1}^{\infty} \|x_{\sigma(n)}\|_{\mathbb{C}_2}^p$ converges.

Hence, $(x_{\sigma(n)}) \in l_p(\mathbb{C}_2)$. Thus, $l_p(\mathbb{C}_2)$ is a bicomplex symmetric space.

Theorem 3.5.[16] The set ω $(\mathbb{C}_2)$ is a linear space over ℝ with respect to addition and scalar multiplication.

Theorem 3.6.[16] The sets $l_\infty(\mathbb{C}_2), c\ (\mathbb{C}_2), c_0\ (\mathbb{C}_2)$ and $l_p\ (\mathbb{C}_2)$ for $0 < p < \infty$ are sequence spaces.

Theorem 3.7. The space $\ell_p\ (\mathbb{C}_2)$ is a complete metric space for $0 < p < \infty$ with the metric $d_{l_p}\ (\mathbb{C}_2)$ defined by

$$d_{l_p(\mathbb{C}_2)}(x,y) = \left\{\sum_{k=1}^{\infty} \|x_k - y_k\|_{\mathbb{C}_2}^p\right\} \text{ for } 0 < p \leq 1$$

$$= \left(\sum_{k=1}^{\infty} \|x_k - y_k\|_{\mathbb{C}_2}^p\right)^{\frac{1}{p}} \text{ for } 1 < p < \infty$$

where $x = (x_k)$, $y = (y_k) \in \ell_p\ (\mathbb{C}_2)$.

Proof.

First, we show that the metric space $\ell_p(\mathbb{C}_2)$ is complete for $1 < p < \infty$.

For this let $(x_m) = (x_k^m)_{k \in \mathbb{N}}$ be any arbitrary Cauchy sequence in the space $\ell_p(\mathbb{C}_2)$. Then, for every $\varepsilon > 0$, there exists $n_o(\varepsilon) \in \mathbb{N}$ such that

$$d(x_m, x_r) = \left(\sum_{k=1}^{\infty} \|x_k^m - x_k^r\|_{\mathbb{C}_2}^p\right)^{\frac{1}{p}} < \infty, \text{for all } m, r \geq no\ (\varepsilon). \quad (1)$$

Then, for any fixed k,

$$\|x_k^m - x_k^r\| < \varepsilon \text{ for all } m, r \geq n_o\ (\varepsilon). \quad (2)$$

Thus, for any fixed k, $(x_k^1, x_k^2, \dots, x_k^m, \dots)$ is a bi-complex Cauchy sequence and so it converges to a point say x_k^* . Collecting the infinitely many limits $(x_1^*, x_2^*, \dots)$, let us define a sequence $x^* = (x_k^*) = (x_1^*, x_2^*, \dots)$.

Then, we show that $x^* = (x_k^*) \in \ell_p\ (\mathbb{C}_2)$ and $x_m \to x^*$ as $m \to \infty$.

By (2), we can write $\|x_k^m - x_k^*\|_{\mathbb{C}_2} \leq \varepsilon$ for all $m \geq n_0(\varepsilon)$, which means that $x_k^m \to x_k^*$ *as* $m \to \infty$. Also from (1), we have

$$\left(\sum_{k=1}^{n} \|x_k^m - x_k^r\|_{\mathbb{C}_2}^p\right)^{\frac{1}{p}} < \varepsilon \text{ for all } m, r \geq n_0\ (\varepsilon).$$

Letting $r \to \infty$, we have $\left(\sum_{k=1}^{n} \|x_k^m - x_k^*\|_{\mathbb{C}_2}^p\right)^{\frac{1}{p}} < \varepsilon$ for all $n \in \mathbb{N}$.

Then by letting $n \to \infty$, we have

$$d(x_m, x^*) = \left(\sum_{k=1}^{\infty} \|x_k^m - x_k^*\|^p\right)^{\frac{1}{p}} \leq \varepsilon \text{ for all } m \geq n_0(\varepsilon).$$

Thus the sequence $(x_m) \in l_p\ (\mathbb{C}_2)$ converges to $x^* = (x_k^*) \in \omega(\mathbb{C}_2)$.

Next, we show that $x^* = (x_k^*) \in \ell_p\ (\mathbb{C}_2)$. Since $(x_m) = (x_k^m) \in \ell_p(\mathbb{C}_2)$, by complex Minkowski's inequality and convergence of the series $\sum_{k=1}^{\infty} \|x_k^* - x_k^m\|_{\mathbb{C}_2}^p$ we have

$$\left(\sum_{k=1}^{\infty}\|x_k^*\|_{\mathbb{C}_2}^p\right)^{\frac{1}{p}} = \left(\sum_{k=1}^{\infty}\|x_k^m + (x_k^* - x_k^m)\|_{\mathbb{C}_2}^p\right)^{\frac{1}{p}}$$

$$\leq \left(\sum_{k=1}^{\infty}\|x_k^m\|_{\mathbb{C}_2}^p\right)^{\frac{1}{p}} + \left(\sum_{k=1}^{\infty}\|x_k^* - x_k^m\|_{\mathbb{C}_2}^p\right)^{\frac{1}{p}} < \infty.$$

Thus $x = (x_k^*) \in l_p$ ($\mathbb{C}_2$). Hence $l_p(\mathbb{C}_2)$ with $1 < p < \infty$ is complete.

Similarly, we can show that ℓ_p $(\mathbb{C}_2)$ is complete for $0 < p \leq 1$ with the metric

$d(x, y) = \sum_{k=1}^{\infty}\|x_k - y_k\|_{\mathbb{C}_2}^p$, where $x = (x_k)$, $y = (y_k) \in \ell_p$ $(\mathbb{C}_2)$.

Since ℓ_p $(\mathbb{C}_2)$ is complete with the metric induced by the norm defined by

$\|x\| = \left\{\sum_{k=1}^{\infty}\|x_k\|_{\mathbb{C}_2}^p\right\}$ for $0 < p \leq 1$.

$= \left(\sum_{k=1}^{\infty}\|x_k\|_{\mathbb{C}_2}^p\right)^{\frac{1}{p}}$ for $1 < p < \infty$

Hence ℓ_p $(\mathbb{C}_2)$is a Banach space.

Theorem 3.8. The space ℓ_p $(\mathbb{C}_2)$ for $0 < p < \infty$ is convex.

Proof.

Let $x = (x_n)$ and $y = (y_n) \in \ell_p$ $(\mathbb{C}_2)$ and $\lambda \in [0,1]$.

Then the series $\sum_{n=1}^{\infty}\|x_n\|_{\mathbb{C}_2}^p$ and $\sum_{n=1}^{\infty}\|y_n\|_{\mathbb{C}_2}^p$ converge.

For $1 < p < \infty$, in view of lemma 2.1, we have

$$\left(\sum_{n=1}^{\infty}\|\lambda\, x_n + (1-\lambda)y_n\|_{\mathbb{C}_2}^p\right)^{\frac{1}{p}} \leq \left(\sum_{n=1}^{\infty}\ \|\lambda\, x_n\|_{\mathbb{C}_2}^p\right)^{\frac{1}{p}} + \left(\sum_{n=1}^{\infty}\|(1-\lambda\,)y_n\|_{\mathbb{C}_2}^p\right)^{\frac{1}{p}}$$

$$= \lambda\left(\sum_{n=1}^{\infty}\|\ x_n\|_{\mathbb{C}_2}^p\right)^{\frac{1}{p}} + (1-\lambda)\left(\sum_{n=1}^{\infty}\|y_n\|_{\mathbb{C}_2}^p\right)^{\frac{1}{p}} < \infty$$

and therefore,

$$\sum_{n=1}^{\infty} \|\ \lambda x_n + (1-\lambda)\ y_n\|^p < \infty.$$

Hence, $\lambda x + (1-\lambda)\, y \in \ell_p$ $(\mathbb{C}_2)$.

Also, for $0 < p \leq 1$, we have by lemma 2.2

$$\sum_{n=1}^{\infty} \|\ \lambda x_n + (1-\lambda)\ y_n\|_{\mathbb{C}_2}^p \leq \sum_{n=1}^{\infty}(\|\lambda\, x_n\|_{\mathbb{C}_2}^p + \|\ (1-\lambda)\ y_n\ \|_{\mathbb{C}_2}^p)$$

$$= \lambda^p \sum_{n=1}^{\infty} \|\ x_n\ \|_{\mathbb{C}_2}^p + (1-\lambda)^p \sum_{n=1}^{\infty}\|y_n\|_{\mathbb{C}_2}^p \quad < \infty.$$

This implies that $\lambda x + (1-\lambda)y \in \ell_p$ $(\mathbb{C}_2)$.

Hence, ℓ_p $(\mathbb{C}_2)$ for $0 < p < \infty$ is convex.

Theorem 3.9. The sequence space $\ell_\infty(\mathbb{C}_2)$is convex.

Proof.

Let $x = (x_n)$, $y = (y_n) \in \ell_\infty(\mathbb{C}_2)$ and $\lambda \in [0,1]$.

Then, $\sup \{\| x_n \|_{\mathbb{C}_2} : n \in \mathbb{N}\} < \infty$ and $\sup \{\| y_n \|_{\mathbb{C}_2} : n \in \mathbb{N}\} < \infty$.

Now, $\sup \{\|\lambda x_n + 1 - \lambda) y_n\|_{\mathbb{C}_2} : n \in \mathbb{N}\} \leq \sup \{\lambda \| x_n \|_{\mathbb{C}_2} : n \in \mathbb{N}\} + (1-\lambda) \| y_n \|_{\mathbb{C}_2} : n \in \mathbb{N}\}$

$= \lambda \sup \{\| x_n \|_{\mathbb{C}_2} : n \in \mathbb{N}\} + (1-\lambda) \sup \{\| y_n \|_{\mathbb{C}_2} : n \in \mathbb{N}\}$

$< \infty$

Thus, $\lambda x + (1-\lambda) y \in \ell_\infty(\mathbb{C}_2)$. Hence, $\ell_\infty(\mathbb{C}_2)$ is convex.

Lemma 3.10. [6] Let p be a real number with $1 < p < \infty$ such that $x \neq y$ where $x = (x_n)$, $y = (y_n)$ and $\lambda \in (0,1)$. Then, we have $\| \lambda x + (1-\lambda) y \|^p < \lambda \|x\|^p_{\mathbb{C}_2} + (1-\lambda) \|y\|^p_{\mathbb{C}_2}$.

Theorem 3.11. The sequence space $\ell_p(\mathbb{C}_2)$ for $1 < p < \infty$ is strictly convex.

Proof.

Let $x = (x_n)$ and $y = (y_n) \in S_{l_p}(\mathbb{C}_2)$ such that $x \neq y$ and $\lambda \in (0,1)$. Then, $\| x \| = 1$ and $\| y \| = 1$.

By lemma 3.10 we have

$\|\lambda x + (1-\lambda) y \|^p_{\mathbb{C}_2} = \sum_{n=1}^{\infty} \| \lambda x_n + (1-\lambda) y_n \|^p \ (\mathbb{C}_2)$

$< \sum_{n=1}^{\infty} [\lambda \| x_n \|^p + (1-\lambda) y_n \|^p \ (\mathbb{C}_2)$

$= \lambda \sum_{n=1}^{\infty} \|x_n\|^p_{\mathbb{C}_2} + (1-\lambda) \sum_{n=1}^{\infty} \|y_n\|^p_{\mathbb{C}_2}$

$= \lambda \ \|x\|^p_{\mathbb{C}_2} + (1-\lambda) \|y\|^p_{\mathbb{C}_2}$

$= \lambda.1 + (1-\lambda).1 = 1$

This shows that $l_p(\mathbb{C}_2)$ for $1 < p < \infty$ is strictly convex.

Example 1. The sequence space $l_1(\mathbb{C}_2)$ is not strictly convex.

Let $x = (x_n) = (0, \ i_1, \ 0, \ 0, \dots \dots)$ and $y = (y_n) = (0, \ 0, -i_2, \ 0, \dots \dots)$
so that $\|x\| = \|y\| = 1$ *and* $\lambda \in (0,1)$.

Now, $\| \lambda x + (1-\lambda) y \|_{l_1(\mathbb{C}_2)} = \sum_{n=1}^{\infty} \| \lambda x_n + (1-\lambda) y_n \|_{(\mathbb{C}_2)}$

$= \sum_{n=1}^{\infty} \|(0, \ \lambda i_1, \ (1-\lambda)(-i_2), \ 0, \dots.) \|$

$= \| \lambda i_1 \|_{\mathbb{C}_2} + \|(1-\lambda)(-i_2)\|_{\mathbb{C}_2}$

$= \lambda.1 + (1-\lambda).1 = 1$, for all $\lambda \in (0,1)$.

Hence $l_1(\mathbb{C}_2)$ is not strictly convex.

Example 2. The sequence space $l_\infty(\mathbb{C}_2)$ is not strictly convex.

Let $x = (x_n) = (1, \ i_1, \ i_2, \ 0, \ 0, \dots)$ and $y = (y_n) = (-1, \ i_1, \ i_2, \ 0, \ 0, \dots)$

Then, $\|x\|_{\mathbb{C}_2} = \|y\|_{\mathbb{C}_2} = 1$.

Now, for all $\lambda \in (0,1)$, we have

$$\|\lambda x + (1-\lambda)\, y\|_{\mathbb{C}_2} = \sup\{\|\lambda x_n + (1-\lambda) y_n\|_{\mathbb{C}_2} : n \in \mathbb{N}\}$$
$$= \sup\{\, \|2\lambda - 1,\ i_1,\ i_2,\ 0,\ 0, \ldots)\,\|_{\mathbb{C}_2} : n \in \mathbb{N}\}$$
$$= \sup\{0,\ |2\lambda - 1|,\ 1\} = 1.$$

Thus $l_\infty(\mathbb{C}_2)$ is not strictly convex.

Theorem 3.12. The sequence space $l_p(\mathbb{C}_2)$ for $2 \le p < \infty$ is uniformly convex.

Proof.

Let $x = (x_n),\ y = y_n \in l_p(\mathbb{C}_2)$ such that

$$\|x\| \le 1,\ \big||y|\big| < 1 \text{ and } \|x - y\| \ge \varepsilon.$$

Then, applying lemma 2.3 we have

$$\|x+y\|^p + \|x-y\|^p = \sum_{n=1}^{\infty}\|x_n + y_n\|^p + \sum_{n=1}^{\infty}\|x_n - y_n\|^p$$
$$= \sum_{n=1}^{\infty}(||x_n + y_n||^p + \|x_n - y_n||^p)$$
$$\le \sum_{n=1}^{\infty} 2^{p-1}\,(||x_n||^p + ||y_n||^p)$$
$$= 2^{p-1}[\sum_{n=1}^{\infty} x_n||^p + \sum_{n=1}^{\infty}\|y_n\|^p]$$
$$= 2^{p-1}[\|x\|^p + \|y\|^p] < 2^{p-1}(1+1)$$
$$= 2^p$$

This shows that $\|x+y\|^p \le 2^p - \|x-y\|^p \le 2^p - \varepsilon^p$.

Now, $\left\|\frac{x+y}{2}\right\| = \left[\frac{1}{2^p}\|x+y\|^p\right]^{\frac{1}{p}}$

$$\le \left[\frac{1}{2^p}(2^p - \varepsilon^p)\right]^{\frac{1}{p}} = \left[1 - (\tfrac{\varepsilon}{2})^p\right]^{\frac{1}{p}}$$

If we take $\delta(\varepsilon) = 1 - \left[1 - \left(\frac{\varepsilon}{2}\right)^p\right]^{\frac{1}{p}}$, then $\left\|\frac{x+y}{2}\right\| \le 1 - \delta$.

Hence $l_p(\mathbb{C}_2)$ for $2 \le p < \infty$ is uniformly convex.

Example 3. The sequence space $l_1(\mathbb{C}_2)$ is not uniformly convex.

Proof.

Let $x = (x_n) = (i_1,\ 0,\ 0,\ 0, \ldots\ldots)$, and $y = (y_n) = (0,\ 0,\ i_2,\ 0, \ldots\ldots)$.Then

$$\|x\| = \|y\| = 1.$$

Now, $\|x - y\|_{\mathbb{C}_2} = \sum_{n=1}^{\infty}\|x_n - y_n\|_{\mathbb{C}_2} = \sum_{n=1}^{\infty}\|(i_1,\ 0, -i_2,\ 0, \ldots.)\|_{\mathbb{C}_2}$

$$= \|i_1\| + \|-i_2\| = 1{+}1 = 2 \ge \varepsilon$$

But $\left\|\frac{x+y}{2}\right\| = \sum_{n=1}^{\infty}\left\|\frac{x_n+y_n}{2}\right\|_{\mathbb{C}_2} = \sum_{n=1}^{\infty}\left\|\frac{1}{2}(i_1,\ 0,\ i_2,\ 0, \ldots)\right\|$

$$= \left\|\frac{i_1}{2}\right\|_{\mathbb{C}_2} + \left\|\frac{i_2}{2}\right\|_{\mathbb{C}_2} = \frac{1}{2} + \frac{1}{2} = 1.$$

Thus, we cannot find $\delta(\varepsilon) > 0$ such that $\left\|\frac{x+y}{2}\right\| \le 1 - \delta$.

Hence, $l_1(\mathbb{C}_2)$ is not uniformly convex.

Example 4. The sequence space $l_\infty(\mathbb{C}_2)$ is not uniformly convex.

Proof.

Let $x = (x_n) = (1,\ i_1,\ i_2,\ 0,\ 0, \ldots), y = (y_n) = (-1,\ i_1,\ -i_2,\ 0,\ 0, \ldots)$

Then, $\|x\| = \|y\| = 1$

$$\|x-y\| = \sup\left\{\|x_n - y_n\|_{\mathbb{C}_2} : n \in \mathbb{N}\right\}$$
$$= \sup\{\|(2,\ 0,\ 2i_2,\ 0,\ 0, \ldots\|\} = \sup\{0, 2\}$$
$$= 2 \geq \varepsilon$$

Now, $$\left\|\frac{x+y}{2}\right\| = \sup\left\{\left\|\frac{x_n+y_n}{2}\right\|_{\mathbb{C}_2} : n \in \mathbb{N}\right\}$$
$$= \sup\left\{\left\|\frac{1}{2}\ (0,\ 2i_1,\ 0,\ 0, \ldots.)\right\|\right\}$$
$$= \sup\{\|(0,\ i_1,\ 0,\ 0, \ldots\|\}$$
$$= \sup\{0, 1\} = 1$$

Thus, we cannot find $\delta(\varepsilon) > 0$ such that $\left\|\frac{x+y}{2}\right\| \leq 1 - \delta$

Hence $l_\infty(\mathbb{C}_2)$ is not uniformly convex.

4. Conclusion

In this paper, we have presented some sequence spaces of bi-complex numbers and their algebraic, topological, and geometric properties. The extension of these properties on generalized double sequences of bi-complex numbers will be the future research directions.

Acknowledgments

The authors would like to acknowledge and offer special thanks to the anonymous referee(s) for their suggestions and comments to improve the paper.

References

[1] Alpay D., Luna Elizarrarás M.E., Shapiro M. & Struppa D. C. (**2014**). Basics of functional analysis with bi-complex scalars and bi-complex Schur analysis, *Springer Science and Business Media*.

[2] Basar F. (**2011**). *Summability Theory and its Applications*, Bentham Science Publishers Istanbul (e - books, Monographs).

[3] Bera. S & Tripathy, B.C. (**2023**). Statistical convergence in bi-complex valued metric space, *Ural Mathematical Journal*, **9** (**1**): 49-63.

[4] Bera. S & Tripathy, B.C. (**2023**). Ceśaro convergence of sequences of bi-complex numbers using BC-Orlicz function, *Filomat*, **37** (**28**): 9769–9775.

[5] Degirmen N. & Sagir B. (**2014**). Some new notes on the bi-complex sequence space $l_p(\mathbb{C}_2)$, *Journal of Fractional Calculus and Applications*, **13** (**2**): 66-76.

[6] Degirmen N. & Sagir B. (**2022**). Some geometric properties of bi-complex sequence spaces, *Konuralp Journal of Mathematics*,**10** (**1**):44- 49.

[7] Ellidokuzoglu H. B. and Demiriz S. (**2018**). Some algebraic and topological properties of new Lucas's difference sequence spaces, *Turk. J. Math. Comput. Sci*., **10:**144- 152.

[8] Ghimire, J.L. & Pahari, N.P.**(2022).** On certain linear structures of Orlicz space $c_0(M,(X, \|.\|), \overline{a}, \overline{\alpha})$ of vector valued difference sequences *The Nepali Mathematical Sciences Report*, **39**(2): 36-44.

[9] Güngör N. (**2020**). Some geometric properties of the non-Newtonian sequence spaces l_p (N), *Math. Slovaca*, **70** (**3**): 689- 696.

[10] Hardy, G.H. (**1917**). On the convergence of certain multiple series, *Proc. Camb. Phil. Soc*., 86-95.

[11] Kumar S. & Tripathy, B. C. (2024). Double Sequences of Bi-complex Numbers, *Proc. Natl. Acad. Sci., India, Sect. A Phys. Sci.,* **16** (**2**):135- 149. https://doi.org/10.1007/s40010-024-00895-7

[12] Pahari, N.P.**(2011)**. On Vector Valued Paranormed Sequence Space $l_\infty(X, ,M, \overline{\lambda}, \overline{p}, L)$ Defined by Orlicz Function, *Nepal Journal of Science Science and Technology*, **12**: 252 – 259.

[13] Paudel, G. P., Pahari, N. P. & Kumar, S. **(2023)**. Topological properties of difference sequence spacethrough Orlicz-paranorm function. *Advances and Applications in Mathematical Sciences*, **22(8)**: 1689-1703.

[14] Pokharel, J. K., Pahari, N. P. & Paudel, G. P. **(2024)**. On topological structure of total paranormed double sequence space $(\ell^2((X, \|.\|), \overline{\gamma}, \overline{w}), G)$, *Journal of Nepal Mathematical Society*, **6(2)**: 53-59.

[15] Price, G. B. (**199**1). *An introduction to Multi-complex Spaces and Function*, M. Dekker.

[16] Pringsheim, A. (**1990**). Zur theotie der zweifach unendlichen zahlenfolgen, *Mathematische Annalen*, **53** (**3**), 289-321.

[17] Rochon, D. & Shapiro, M. (**2004**). On algebraic properties of bi-complex and hyperbolic numbers, *Anal. Univ. Oradea, fasc. Math*., **11**: 1-28.

[18] Sager, N. & Sagir, B. (**2020**). On the completeness of some bi-complex sequence spaces, *Palestine Journal of Mathematics*, **9** (**2**): 891-902.

[19] Segre, C. (**1892**). Le rappresenttazioni reali delle forme complessee gli enti iperal gebrici, *Math. Ann*., **40** (**3**): 413-467.

[20] Srivastava, J.K. & Pahari, N.P.**(2012)**. On vector valued paranormed sequence space $c_0(X, M, \overline{\lambda}, \overline{p})$ defined by Orlicz function. *J. Rajasthan Acad. of Phy. Sci*.,**11(2)**:11-24.

[21] Srivastava, R. K. & Srivastava, N. K. (**2007**). On a class of entire bi-complex sequences, *Southeast Asian J. Math. & Math. Sc*., **5** (**3**): 47-68.

[22] Wagh, M. A. (**2014**). On certain spaces of bi-complex sequences, *Inter. Jour. Phy., Chem. And Math. Fund*, **7** (**1**): 1-6.

Nepal Journal of Mathematical Sciences (NJMS)
ISSN: 2738-9928 (online), 2738-9812 (print)
Vol. 6, No. 1, 2025 (February): 45-50
DOI:10.3126/njmathsci.v6i1.77377

Research Article
Received Date: January 20, 2025
Accepted Date:March 26, 2025
Published Date: April 8, 2025

Extension of Hermite-Hadamard Type Integral Inequality for m-Convex Functions with Second Order Derivatives

Pitamber Tiwari[1*] & Chet Raj Bhatta [2]

[1] *Department of Mathematics, Tribhuvan University, Bhairahawa Multiple Campus, Siddharthanagar, Nepal*

[2] *Central Department of Mathematics, Tribhuvan University, Kirtipur, Kathmandu, Nepal*

Corresponding Author: [*]pitambar.tiwari@bmc.tu.edu.np

Abstract: *Integral inequality is a fascinating research domain that helps to estimate the integral mean of convex functions. The convexity theory plays a basic role in the development of various branches of applied sciences. Convexity and inequality are connected which has a fundamental character in many branches of pure and applied disciplines. The Hermite-Hadamard (H-H) type integral inequality is one of the most important inequalities associated with the convex functions. The researchers are being motivated to the extensions, enhancements and generalizations of H-H type inequality for different types of convex functions. In this paper, we have obtained an extension of some integral inequalities of Hermite-Hadamard type for m-convex functions with second order derivatives on the basis of the classical convex functions.*

Keywords: Convexity, m-convexity, integral inequality

1. Introduction

Convexity theory is essential in the theoretical aspects of mathematicians, economists, and physicists. Mathematicians utilize this theory to solve difficulties that emerge in several subjects of study. Convex analysis has played a pivotal role in the generalizations and extensions of inequalities theory over the last few decades. The theories of convexity and inequality are closely connected. Integral inequalities are important and valuable in information technology, integral operator theory, numerical integration, optimization theory, statistics, probability, and stochastic processes because they are elegant and effective. Many mathematicians and research academics have focused their efforts and contributions over the last few decades on studying these types of inequalities. Thus, for convexity, there is vast and important literature on inequalities. Convexity is a broad subject that also includes the theory of convex functions. Convexity is a powerful property of functions, also known as a natural property of functions. Furthermore, its minimization property makes it unique, novel, and beneficial. Due to its minimization characteristic, it possesses a significant status in optimization theory, calculus of variation, and probability theory. So, the idea of convex functions has played a significant role in modern mathematics [2]. It has been noticed that several books and research articles have been published in the past few years. The H-H inequality substantially impacted the study of a convex function [1]. Numerous important inequalities have been employed as powerful tools not only in pure mathematics but also in other areas of mathematics, for if, the theory of means, approximation theory, numerical analysis, and so on. One of the most important inequalities that has been attracted by many inequality experts in the last few decades is the famous Hermite-Hadamard inequality. Although, it was firstly known in literature as a result of J. Hadamard in 1893, but this result was actually due to C. Hermite in 1881, as pointed out by Mitrinovic and Lacovic [3] in 1985. Due to this fact, most experts refer to it as Hermite-Hadamard (or sometimes, Hadamard-Hermite) inequality which is defined as follows:

Let $f : [a,b] \subset \mathbb{R} \to \mathbb{R}$ be a convex function, where $x, y \in [a,b]$ with $x < y$. Then, the following inequalities hold:

$$f\left(\frac{x+y}{2}\right) \leq \frac{1}{y-x}\int_{x}^{y} f(x)\,dx \leq \frac{f(x)+f(y)}{2} \tag{1}$$

The result in equation (1) is considered as a necessary and a sufficient condition for a function $f : [a,b] \subset \mathbb{R} \to \mathbb{R}$ be a convex function. This famous inequality has raised attention of the researchers of the domain of convexity and inequality theory and a variety of refinements and generalizations have been found in it. This classical Hermite-Hadamard integral inequality estimates the integral mean value of a continuous convex function $f : [a,b] \to \mathbb{R}$. The extensions of Hermite-Hadamard type integral inequalities in recent years have taken a significant growth. Tiwari and Bhatta [6] have extended the Hermite-Hadamard type integral inequality of classical convex functions to m-convex functions whose the first order derivatives are m-convex functions and some results are proved in the framework of $q-$calculus. The present paper incorporates four sections. The first section includes the concept of convex functions and its applications in different streams along with the Hermite-Hadamard integral inequality. The second section includes the definition of classical convex function as well as its extension to m-convex function. It also incorporates the result of H-H type integral inequality whose second order derivatives are convex functions. The third section highlights the main results of the research, and it concludes in the fourth section by explaining the research domain to the future researchers.

2. Preliminary Results

The concept of convex function in classical sense is defined as follows:

Definition 2.1. The function $f : [a,b] \subset \mathbb{R} \to \mathbb{R}$ is said to be convex if the following inequality

$$f(\lambda x + (1-\lambda)y) \leq \lambda f(x) + (1-\lambda)f(y) \tag{2}$$

holds for all $x, y \in [a,b], \lambda \in [0,1]$. We say that that f is concave if $(-f)$ is convex.

G. H. Toader [5] introduced the idea of m-convexity of the function, an intermediate between the usual convexity and the star shaped property as follows:

Definition 2.2. The function $f : [0,b] \to \mathbb{R}$ is said to be m-convex function where $m \in [0,1]$ for every $x, y \in [0,b]$ and $\lambda \in [0,b]$, we have

$$f(\lambda x + m(1-\lambda)y) \leq \lambda f(x) + m(1-\lambda)f(y).$$

Remark 2.3. For $m = 1$, we recapture the concept of convex functions on $[0,b]$ and for $m = 0$, we get the concept of star shaped functions on $[0,b]$. We recall that $f : [0,b] \to \mathbb{R}$ is star shaped if

$$f(\lambda x) \leq \lambda f(x)$$

for all $\lambda \in [0,b]$ and $x \in [0,b]$.

Odzemir et al. [4] proved the following result for the case of classical convex function.

Theorem 2.4. *Let $f : I \subset \mathbb{R} \to \mathbb{R}$ be a twice differentiable mapping on $I^0, x, y \in I$ with $x < y$ and f'' be integrable on $[x,y]$, then the following equality holds:*

$$\frac{f(x)+f(y)}{2} - \frac{1}{y-x}\int_x^y f(s)\,ds = \frac{(y-x)^2}{2}\int_0^1 \lambda(1-\lambda)f''(\lambda x + (1-\lambda)y)\,d\lambda$$

3. Main Results

In this section, we extend the idea of H-H type integral inequality of second order differentiable classical convex functions to m-convex functions as follows:

Lemma 3.1. *Let $f : I \subset \mathbb{R} \to \mathbb{R}$ be a twice differentiable mapping on I^0 where $x, y \in I$ with $x < y$, I^0 is an interior of I and $m \in [0,1]$. If $f'' \in L([x,y])$, then the following equality holds:*

$$\frac{f(x)+f(my)}{2}-\frac{1}{my-x}\int_x^{my} f(u)\,du=\frac{(my-x)^2}{2}\int_0^1 \lambda(1-\lambda)f''(\lambda x+m(1-\lambda)y)\,d\lambda$$

Proof.

$$\begin{aligned} Let \quad I_1 &= \int_0^1 \lambda(1-\lambda)f''(\lambda x+m(1-\lambda)y)\,d\lambda \\ &= \int_0^1 (\lambda-\lambda^2)f''(\lambda x+m(1-\lambda)y)\,d\lambda \end{aligned}$$

Integrating by parts, we have

$$\begin{aligned} &= \left[(\lambda-\lambda^2)\frac{f'(\lambda x+m(1-\lambda)y)}{x-my}\right]_0^1 - \int_0^1 (1-2\lambda)f'\frac{(\lambda x+m(1-\lambda)y)}{x-my}\,d\lambda \\ &=0-\int_0^1 (1-2\lambda)f'\frac{(\lambda x+m(1-\lambda)y)}{x-my}\,d\lambda \\ &=\frac{1}{my-x}\int_0^1 (1-2\lambda)f'(\lambda x+m(1-\lambda)y)\,d\lambda \end{aligned}$$

Again integrating by parts, we obtain

$$\begin{aligned} &=\frac{1}{my-x}\left[(1-2\lambda)\frac{f(\lambda x+m(1-\lambda)y)}{x-my}|_0^1-\int_0^1 2\frac{(\lambda x+m(1-\lambda)y)}{x-my}\,d\lambda\right] \\ &=\frac{1}{my-x}\left[\frac{(-1)f(x)}{x-my}-\frac{f(my)}{x-my}+\frac{2}{x-my}\int_0^1 f(\lambda x+m(1-\lambda)y)\,d\lambda\right] \\ &=\frac{1}{my-x}\left[\frac{f(x)+f(my)}{my-x}-\frac{2}{my-x}\int_0^1 f(\lambda x+m(1-\lambda)y)\,d\lambda\right] \\ &=\frac{f(x)+f(my)}{(my-x)^2}-\frac{2}{(my-x)^2}\int_0^1 f(\lambda x+m(1-\lambda)y)\,d\lambda \end{aligned}$$

Put $u=\lambda x+m(1-\lambda)y$. When $\lambda=0$, then $u=my$, when $\lambda=1$, then $u=x$. Also, $d\lambda=-\frac{du}{my-x}$. On substituting these values in the above relation, we get

$$\begin{aligned} \int_0^1 \lambda(1-\lambda)f''(\lambda x+m(1-\lambda)y)\,d\lambda &=\frac{f(x)+f(my)}{(my-x)^2}-\frac{2}{(my-x)^2}\int_{my}^{x} f(u)\frac{(-du)}{my-x} \\ \int_0^1 \lambda(1-\lambda)f''(\lambda x+m(1-\lambda)y)\,d\lambda &=\frac{2}{(my-x)^2}\left[\frac{f(x)+f(my)}{2}-\frac{1}{my-x}\int_x^{my} f(u)\,du\right] \\ \frac{f(x)+f(my)}{2}-\frac{1}{my-x}\int_x^{my} f(u)\,du &=\frac{(my-x)^2}{2}\int_0^1 \lambda(1-\lambda)f''(\lambda x+m(1-\lambda)y)\,d\lambda. \end{aligned}$$

Remark 3.2. If $m=1$, then this result reduces to theorem 2.4.

Theorem 3.3. *Let $f: I\subset\mathbb{R}\to\mathbb{R}$ be a twice differentiable mapping on I^0 where $x,y\in I$ with $x<y$, I^0 is*

an interior of I and $m \in [0,1]$. If $f'' \in L[x,y]$, then the following inequality holds:

$$\left|\frac{f(x)+f(my)}{2} - \frac{1}{my-x}\int_x^{my} f(u)\,du\right| \leq \frac{(my-x)^2}{64}\left(m|f''(y)|+|f''(x)|\right)$$

Proof. Using the result of 3.1 and taking modulus on both sides, we have

$$\begin{aligned}\left|\frac{f(x)+f(my)}{2} - \frac{1}{my-x}\int_x^{my} f(u)\,du\right| &= \left|\frac{(my-x)^2}{2}\int_0^1 \lambda(1-\lambda)f''(\lambda a+m(1-\lambda)y)\,d\lambda\right| \\ &\leq \frac{(my-x)^2}{2}\int_0^1 |\lambda-\lambda^2||f''(\lambda x+m(1-\lambda)y)|\,d\lambda \\ \leq \frac{(my-x)^2}{2}\bigg[|f''(x)|\int_0^1 \lambda|\lambda-\lambda^2|\,d\lambda &+ m|f''(y)|\int_0^1 (1-\lambda)|\lambda-\lambda^2|\,d\lambda\bigg]\end{aligned}$$

Here

$$\int_0^1 \lambda|\lambda-\lambda^2|\,d\lambda = \int_0^{\frac{1}{2}} \lambda(\lambda-\lambda^2)\,d\lambda + \int_{\frac{1}{2}}^1 \lambda(\lambda^2-\lambda)\,d\lambda = \frac{1}{32}$$

And,

$$\int_0^1 (1-\lambda)|\lambda-\lambda^2|\,d\lambda = \int_0^{\frac{1}{2}} (1-\lambda)(\lambda-\lambda^2)\,d\lambda + \int_{\frac{1}{2}}^1 (1-\lambda)(\lambda^2-\lambda)\,d\lambda = \frac{1}{32}$$

Substituting these values, we obtain

$$\left|\frac{f(x)+f(my)}{2} - \frac{1}{my-x}\int_x^{my} f(u)\,du\right| \leq \frac{(my-x)^2}{64}\left(m|f''(y)|+|f''(x)|\right)$$

The proof is complete.

4. Conclusion

The Hermite-Hadamard integral inequality yields the lower and upper bounds of integral mean of any convex function. In this paper, we have extended the results of classical convex function into an m-convex function whose second order derivatives are m-convex functions. The interested researchers can enhance the H-H type integral inequality for other types of convex functions.

References

[1] Beckenbach, E.F., Bellman, R., & Bellman, R.E. **(1961)**. An introduction to inequalities. Technical report, *Mathematical Association of America Washington, DC*.

[2] Gardner, R. **(2002)**. The brunn-minkowski inequality, *Bulletin of the American mathematical society*, **39(3):** 355-405.

[3] Mitrinovic, D. S. & Lakovic, I. B. **(1985)**. Hermite and Convexity, *Aequationes, Math.*, **28(3):** 229-232.

[4] Özdemir, M. E., Avci, M. & Set E. **(2010)**. On some inequalities of Hermite–Hadamard type via -convexity *Appl. Math. Lett.*, **23(9):** 1065-1070.

[5] Toader, G. **(1985)**. Some generalizations of the convexity, proceedings of the Colloquium on Approximation and Optimization, *Univ. Cluj-Napoca*, 329-338.

[6] Tiwari, P. & Bhatta, C. R. **(2023)**. Hermite-Hadamard inequality whose first order q-derivatives are m-convex functions, *Adv. Appl. Math. Sci.*, **22(11):** 2171-2188.

Nepal Journal of Mathematical Sciences (NJMS)
ISSN: 2738-9928 (online), 2738-9912 (print)
Vol. 6, No. 1, 2025 (February): 51–60
DOI://doi.org/10.3126/njmathsci.v6i1.77378

Research Article
Received Date: February 8, 2025
Accepted Date:March 25, 2025
Published Date: April 8, 2025

Interpolative Contraction and Discontinuity at Fixed Point on Partial Metric Spaces

Nabaraj Adhikari*

Central Department of Mathematics, Tribhuvan University, Kirtipur, Kathmandu, Nepal

Corresponding Author: *nabaraj.adhikari@cdmath.tu.edu.np

Abstract: *This paper proposes a novel technique for solving Rhodes' discontinuity problem by exploiting the features of a self-mapping that has a fixed point but is not continuous at that point within a partial metric space. Moreover, we investigate some geometric properties of F_T under interpolative-type contractions and establish a few results related to fixed-discs and fixed-circles.*

Keywords: *Fixed point, Partial metric, Interpolative contraction*

1. Introduction

The Banach contraction principle [4] is a classical result that ranks among the most commonly used and cited fixed point theorems. It states that if a self-mapping T on a complete metric space (X,d) satisfies the condition

$$d(Tx,Ty) \leq a\, d(x,y)$$

for all $x,y \in X$ with $0 \leq a < 1$, then T has a unique fixed point $x^* \in X$. It is well established that the Banach contraction mapping T is continuous over the entire domain X. Kannan [8] proved that there are contractive mappings with fixed points that may not be continuous across the entire domain.

Theorem 1.1. *[8] Let (X,d) be a metric space that is complete, and let $T : X \to X$ be a self-map. If T satisfies the Kannan contraction condition*

$$d(Tx,Ty) \leq b\,[d(x,Tx) + d(y,Ty)], \quad 0 \leq b < \tfrac{1}{2}$$

for all $x,y \in X$ then T admits a unique fixed point in X.

Kannan's contraction mapping is known to be continuous at its fixed point. In [17], Rhoades questioned whether a contractive condition could be formulated that guarantees the existence of a fixed point without assuming the continuity of the mapping at that point. This unresolved problem has motivated several attempts and contributions over time. Using the function $m(x,y) = \max\{d(x,Tx), d(y,Ty)\}$, Pant [16] found an initial solution in the metric space (X,d). Later, Bist and Pant [5] proposed another solution to this open problem.

Erdal Karapinar, a distinguished mathematician, introduced the notion of "interpolative contraction" in metric spaces in his work [9]. The interpolation approach has proven useful in exploring a wide range of classical and modern contraction types (see [3], [5], [7], [10], [14] for further details). More recently, Tas [19] addressed Rhoades' discontinuity problem by presenting a novel solution involving the existence of a fixed point for a self-map that is not continuous at that point. This was achieved by adapting the concepts of interpolative Boyd-Wong contractions and interpolative Matkowski-type contractions as follows:

Theorem 1.2. *[19] Let (X,d) be a complete metric space. Let $T : X \to X$ be a self-map such that for all $x, y \in X$ and $\varepsilon > 0$, there exists $\delta(\varepsilon) > 0$ such that*

$$\varepsilon \leq n(x,y) < \varepsilon + \delta(\varepsilon) \implies d(Tx,Ty) < \varepsilon.$$

If T is $k-$ continuous then T has a unique fixed point say z. Moreover, T is continuous at z if and only if

$$\lim_{x \to z} n(x,z) = 0,$$

where

$$n(x,y) = [d(x,y)]^{\beta}[d(x,Tx)]^{\alpha}[d(y,Ty)]^{\gamma}\left[\frac{d(x,Ty)+d(y,Tx)}{2}\right]^{1-\alpha-\beta-\gamma}$$

and $\alpha, \beta, \gamma \in (0,1)$ with $\alpha+\beta+\gamma < 1$.

Matthews [12] introduced partial metric spaces as a tool for investigating the denotational semantics of data flow networks and extended the classical Banach contraction principle to this more general setting of complete partial metric spaces. Subsequently, Karapinar, Alqahtani, and Aydi [11] explored a Hardy-Rogers type interpolative contraction and established a fixed point theorem within the framework of complete partial metric spaces.
In this work, we propose a revised form of the interpolative Boyd-Wong contraction and the Matkowski-type contraction, building upon the findings of and extending them within the setting of partial metric spaces.

2. Preliminaries

Consider a nonempty set X. The notations $\mathbb{R}$, $\mathbb{R}^+$, and $\mathbb{N}$ stand for the set of real numbers, the set of positive real numbers, and the set of natural numbers, respectively. In [12], Matthews introduced the definition of a partial metric as follows:

Definition 2.1 ([12]). A partial metric on a nonempty set X is a function $p : X \times X \to [0,\infty)$ that satisfies the following conditions for all $x, y, z \in X$:

(P1) $p(x,x) = p(y,y) = p(x,y)$ if and only if $x = y$;

(P2) $0 \leq p(x,x) \leq p(x,y)$;

(P3) $p(x,y) = p(y,x)$;

(P4) $p(x,y) \leq p(x,z) + p(z,y) - p(z,z)$.

A partial metric space is a pair (X, p) such that X is a nonempty set and p is a partial metric on X. A partial metric becomes a metric if $p(x,x) = 0$ for every $x \in X$.

Definition 2.2 ([12]). Let (X, p) be a partial metric space, a point $x_0 \in X$ and $\varepsilon > 0$. The open ball for a partial metric p is set of the form

$$B_{\varepsilon}(x_0) = \{x \in X : p(x_0,x) < p(x_0,x_0) + \varepsilon\}.$$

In contrast to metric spaces, some open balls may be empty in partial metric spaces. For each partial metric p on X, a topology τ_p is induced on X, where the family of open p-balls

$$\{B_\varepsilon(x) : x \in X, \varepsilon > 0\}$$

forms a basis. These open p-balls are defined by

$$B_\varepsilon(x) = \{y \in X : p(x,y) < p(x,x) + \varepsilon\}$$

for all $x \in X$ and $\varepsilon > 0$. If p is a partial metric on X, then the function $d_p : X \times X \to [0,\infty)$ defined by

$$d_p(x,y) = 2p(x,y) - p(x,x) - p(y,y)$$

is a metric on X.

Definition 2.3 ([12]). Let (X,p) be a partial metric space and $\{x_n\}$ be a sequence in X.

(i) $\{x_n\}$ converges to a point $x \in X$ if $p(x,x) = \lim_{n\to\infty} p(x,x_n)$.

(ii) $\{x_n\}$ is called a Cauchy if and only if $\lim_{n,m\to\infty} p(x_n,x_m)$ exists.

(ii) A partial metric space (X,p) is said to be complete if every Cauchy sequence $\{x_n\}$ in X converges, with respect to τ_p, to a point $x \in X$, such that

$$p(x,x) = \lim_{n,m\to\infty} p(x_n,x_m) = \lim_{n\to\infty} p(x_n,x).$$

Lemma 2.4 ([12]). *Let (X,p) be partial metric space and $\{x_n\}$ be a sequence in X. Then*

(i) $\{x_n\}$ is a Cauchy in (X,p) if and only if it is Cauchy in (X,d_p).

(ii) (X,p) is complete if and only if (X,d_p) is complete.

(iii) $\lim_{n\to\infty} d_p(x_n,x) = 0$ if and only if $p(x,x) = \lim_{n,m\to\infty} p(x_n,x_m) = \lim_{n\to\infty} p(x_n,x)$.

3. Main Results

In the following sequel, we denote

$$A(x,y) = [p(x,y)]^\beta \ [p(x,Tx)]^\alpha [p(y,Ty)]^\gamma \ \left[\frac{p(x,Ty)+p(y,Tx)}{2}\right]^{1-\alpha-\beta-\gamma}$$

where $\alpha,\beta,\gamma \in (0,1)$ with $\alpha+\beta+\gamma < 1$.

Theorem 3.1. *Let (X,p) be a complete partial metric space. Let $T : X \to X$ be a self-map. For a given $\varepsilon > 0$, there exists $\delta(\varepsilon) > 0$ such that*

$$\varepsilon \le A(x,y) < \varepsilon + \delta(\varepsilon) \implies p(Tx,Ty) < \varepsilon$$

for all $x,y \in X$. Then the sequence $\{T^n x\}$ is a Cauchy sequence and $\lim_{n\to\infty} p(T^n x,z) = p(z,z)$ for some $z \in X$.

Proof. Suppose $A(x,y) > 0$. Then

$$p(Tx,Ty) < \varepsilon \leq A(x,y) \implies p(Tx,Ty) < A(x,y). \tag{1}$$

Let $x_0 \in X$. Define a sequence $\{x_n\}$ in X by

$$x_{n+1} = Tx_n = T^n x_0$$

and

$$q_n = p(x_n, x_{n+1})$$

for all $n \in \mathbb{N} \cup \{0\}$. Suppose $x_n \neq x_{n+1}$ for each n. Then by inequality (1), we have

$$\begin{aligned}
q_n = p(x_n,x_{n+1}) =& p(Tx_{n-1},Tx_n)\\
&< A(x_{n-1},x_n)\\
&= [p(x_{n-1},x_n)]^{\beta}[p(x_{n-1},Tx_{n-1})]^{\alpha}[p(x_n,Tx_n)]^{\gamma}\left[\frac{p(x_{n-1},Tx_n)+p(x_n,Tx_{n-1})}{2}\right]^{1-\alpha-\beta-\gamma}\\
&= [p(x_{n-1},x_n)]^{\beta}[p(x_{n-1},x_n)]^{\alpha}[p(x_n,x_{n+1})]^{\gamma}\left[\frac{p(x_{n-1},x_{n+1})+p(x_n,x_n)}{2}\right]^{1-\alpha-\beta-\gamma}\\
&\leq [p(x_{n-1},x_n)]^{\beta+\alpha}[p(x_n,x_{n+1})]^{\gamma}\left[\frac{p(x_{n-1},x_n)+p(x_n,x_{n+1})}{2}\right]^{1-\alpha-\beta-\gamma}\\
&= q_{n-1}^{\alpha+\beta} q_n^{\gamma}\left[\frac{q_{n-1}+q_n}{2}\right]^{1-\alpha-\beta-\gamma}.
\end{aligned}$$

Therefore,

$$q_n < q_{n-1}^{\alpha+\beta} q_n^{\gamma} \left[\frac{q_{n-1}+q_n}{2}\right]^{1-\alpha-\beta-\gamma}. \tag{2}$$

Again, suppose $q_{n-1} < q_n$ for some $n \in \mathbb{N}$. Then we have

$$\frac{q_{n-1}+q_n}{2} < q_n.$$

From inequality (2) we get

$$\begin{aligned}
& q_n < [q_{n-1}]^{\alpha+\beta}[q_n]^{\gamma}[q_n]^{1-\alpha-\beta-\gamma}\\
\implies & q_n < [q_{n-1}]^{\alpha+\beta}[q_n]^{1-\alpha-\beta}\\
\implies & q_n^{\alpha+\beta} < q_{n-1}^{\alpha+\beta}\\
\implies & q_n < q_{n-1}
\end{aligned}$$

which is a contradiction of our assumption. Therefore, $q_n \leq q_{n-1}$ for all $n \in \mathbb{N}$. We come to the conclusion that the s $\{q_{n-1}\}$ is decreasing and contains real numbers that are not negative. Therefore, a non-negative constant q exists such that $\lim_{n\to\infty} q_{n-1} = q$. Since $q_n \leq q_{n-1}$, so

$$\frac{q_{n-1}+q_n}{2} \leq q_{n-1}$$

for all $n \geq 1$. Using the inequality (2) we have

$$\begin{aligned}
& q_n < [q_{n-1}]^{\alpha+\beta}[q_n]^{\gamma}[q_{n-1}]^{1-\alpha-\beta-\gamma}\\
\implies & q_n < [q_{n-1}]^{1-\gamma}[q_n]^{\gamma}\\
\implies & q_n < q_{n-1}\\
\therefore & \lim_{n\to\infty} q_n = q < \lim_{n\to\infty} q_{n-1} = q.
\end{aligned}$$

which is contradiction. Hence, $q = 0$.
i.e.,

$$\lim_{n\to\infty} q_n = \lim_{n\to\infty} p(x_n, x_{n+1}) = 0.$$

Now, we show that $\{x_n\}$ is a Cauchy sequence in (X, p). If possible suppose $\{x_n\}$ is not Cauchy sequence. As a result, one can find a positive constant $\varepsilon > 0$ and two sub-sequences $\{x_{m_k}\}$ and $\{x_{n_k}\}$ of $\{x_n\}$ such that

$$m_k > n_k > k \quad \text{and} \quad p(x_{m_k}, x_{n_k}) \geq \varepsilon \tag{3}$$

Choosing the smallest m_k satisfying (3). So, $p(x_{n_k}, x_{m_k-1}) < \varepsilon$. Consider any $k \in \mathbb{N}$. Then,

$$\begin{aligned}\varepsilon \leq p(x_{m_k}, x_{n_k}) &\leq p(x_{m_k}, x_{m_k-1}) + p(x_{m_k-1}, x_{n_k}) - p(x_{m_k-1}, x_{m_k-1}) \\ &\leq p(x_{m_k}, x_{m_k-1}) + p(x_{m_k-1}, x_{n_k}) \\ &< \varepsilon + p(x_{m_k}, x_{m_k-1}).\end{aligned}$$

Therefore,

$$\varepsilon \leq p(x_{m_k}, x_{n_k}) < \varepsilon + p(x_{m_k}, x_{m_k-1}). \tag{4}$$

Taking limit $k \to \infty$ in (4)

$$\begin{aligned}\varepsilon \leq \lim_{k\to\infty} p(x_{m_k}, x_{n_k}) &< \varepsilon + \lim_{k\to\infty} p(x_{m_k}, x_{m_k-1}) \\ \Rightarrow \varepsilon \leq \lim_{k\to\infty} p(x_{m_k}, x_{n_k}) &< \varepsilon \\ \Rightarrow \lim_{k\to\infty} p(x_{m_k}, x_{n_k}) &= \varepsilon.\end{aligned}$$

Using (P4) and above relation we have $\lim_{k\to\infty} p(x_{m_{k+1}}, x_{n_{k+1}}) = \varepsilon$. Again, we have

$$\begin{aligned}p(x_{n_k+1}, x_{m_k+1}) &= p(Tx_{n_k}, Tx_{m_k}) \\ &< A(x_{n_k}, x_{m_k}) \\ &= [p(x_{n_k}, x_{m_k})]^{\beta} [p(x_{n_k}, Tx_{n_k})]^{\alpha} [p(x_{m_k}, Tx_{m_k})]^{\gamma} \left[\frac{p(x_{n_k}, Tx_{m_k}) + p(x_{m_k}, Tx_{n_k})}{2}\right]^{1-\alpha-\beta-\gamma} \\ &= [p(x_{n_k}, x_{m_k})]^{\beta} [p(x_{n_k}, x_{n_k+1})]^{\alpha} [p(x_{m_k}, x_{m_k+1})]^{\gamma} \left[\frac{p(x_{n_k}, x_{m_k+1}) + p(x_{m_k}, x_{n_k+1})}{2}\right]^{1-\alpha-\beta-\gamma}\end{aligned}$$

$$\Rightarrow \lim_{n\to\infty} p(x_{n_k+1}, x_{m_k+1}) < 0$$

which contradicts the assumption. Therefore $\{x_n\}$ is a Cauchy sequence in the complete partial metric space (X, p). Hence, $\lim_{n\to\infty} p(T^n x, z) = p(z, z)$ for some $z \in X$. □

Definition 3.2. Let (X, p) be a partial metric space . A self-map $T : X \to X$ is called $k-$continuous, $k = 1, 2, 3, \cdots$, if $\lim_{n\to\infty} p(T^k x_n, x) = p(Tx, Tx)$ whenever $\{x_n\}$ is a sequence in X such that

$$\lim_{n\to\infty} p(T^{k-1} x_n, x) = p(x, x).$$

It was established in [15] that for $k > 1$, the notions of continuity of T^k and k-continuity of T are not dependent on each other within metric spaces. This conclusion is also applicable within the framework of partial metric spaces. Clearly, 1-continuity is just another way of stating continuity. Furthermore, there exists a one-way chain of implications:

$$\text{continuity} \Rightarrow \text{2-continuity} \Rightarrow \text{3-continuity} \Rightarrow \cdots,$$

though the reverse implications do not generally hold.

Theorem 3.3. *Let (X,p) be a complete partial metric space. Let $T: X \to X$ be a self-map such that for all $x,y \in X$ and $\varepsilon > 0$, there exists $\delta(\varepsilon) > 0$ such that*

$$\varepsilon \le A(x,y) < \varepsilon + \delta(\varepsilon) \implies p(Tx,Ty) < \varepsilon. \tag{5}$$

If T is k-continuous, then it admits a fixed point z. Moreover, T is continuous at z if and only if

$$\lim_{x\to z} A(x,z) = p(z,z).$$

Proof. Let $x_0 \in X$, and construct a Picard sequence $\{x_n\}$ in X by setting

$$x_{n+1} = Tx_n = T^n x_0.$$

According to Theorem 3.1, the sequence $\{x_n\}$ is Cauchy. As (X,p) is a complete metric space, there exists a point $z \in X$ satisfying

$$\lim_{n\to\infty} p(x_n,z) = p(z,z).$$

i.e.,

$$\lim_{n\to\infty} p(T^n x,z) = p(z,z).$$

Since T is $k-$continuous then

$$\lim_{n\to\infty} p(T^{k-1}x_n,z) = p(z,z) \Rightarrow \lim_{n\to\infty} p(T^k x_n,Tz) = p(Tz,Tz).$$

Therefore,

$$p(z,z) = p(Tz,Tz).$$

So by (P1) $Tz = z$. Consequently, z is a point that remains fixed under T.
Assume that T is continuous at the fixed point z. and $\lim_{n\to\infty} p(x_n,z) = p(z,z)$. Then

$$\lim_{n\to\infty} p(Tx_n,Tz) = p(Tz,Tz) = p(z,z).$$

Hence

$$\begin{aligned}
\lim_{x\to z} A(x,z) =& \lim_{x\to z}\left[[p(x,z)]^{\beta}[p(x,Tx)]^{\alpha}[p(z,Tz)]^{\gamma}\left(\frac{p(x,Tz)+p(z,Tx)}{2}\right)^{1-\alpha-\beta-\gamma}\right] \\
=& [p(z,z)]^{\beta}[p(z,Tz)]^{\alpha}[p(z,Tz)]^{\gamma}\left(\frac{p(z,Tz)+p(z,Tz)}{2}\right)^{1-\alpha-\beta-\gamma} \\
=& p(z,z).
\end{aligned}$$

Conversely, suppose $\lim_{x\to z} A(x,z) = p(z,z)$. Let $\lim_{n\to\infty} p(x_n,z) = p(z,z)$. Then

$$\begin{aligned}
&\text{``}\lim_{x\to z} A(x,z) = p(z,z) \\
\Rightarrow \lim_{x\to z}\left[[p(x,z)]^{\beta}[p(x,Tx)]^{\alpha}[p(z,Tz)]^{\gamma}\left(\frac{p(x,Tz)+p(z,Tx)}{2}\right)^{1-\alpha-\beta-\gamma}\right] &= p(z,z) \\
\Rightarrow [p(z,z)]^{\beta}\lim_{x\to z}[p(x,Tx)]^{\alpha}[p(z,z)]^{\gamma}\left(\frac{p(z,z)+p(z,z)}{2}\right)^{1-\alpha-\beta-\gamma} &= p(z,z) \\
\Rightarrow [p(z,z)]^{1-\alpha}\lim_{x\to z}[p(x,Tx)]^{\alpha} &= p(z,z) \\
\Rightarrow \lim_{x\to z}[p(x,Tx)]^{\alpha} &= [p(z,z)]^{\alpha} \\
\Rightarrow \lim_{x\to z}[p(x,Tx)] &= [p(z,z)] \\
\Rightarrow \lim_{x\to z}[p(Tx,Tz)] &= p(Tz,Tz).
\end{aligned}$$

Hence T is continuous. □

Definition 3.4. [1] Let Ψ be the class of all functions $\phi : [0,\infty) \to [0,\infty)$ that satisfy the following requirements:

(i) ϕ is non-decreasing; that is, for any $\alpha_1 < \alpha_2$, we have $\phi(\alpha_1) \leq \phi(\alpha_2)$;

(ii) ϕ is continuous;

(iii) For every $\alpha > 0$, the series $\sum_{n=1}^{\infty} \phi^n(\alpha)$ converges.

Corollary 3.5. *Let (X, p) be a complete partial metric space, and let $T : X \to X$ be a self-map such that for all $x, y \in X$, the following conditions are satisfied:*

(i) $\forall\, \varepsilon > 0, \exists\, \delta(\varepsilon) > 0 : \varepsilon \leq A(x,y) < \varepsilon + \delta(\varepsilon) \Rightarrow p(Tx, Ty) < \varepsilon.$

(ii) $p(Tx, Ty) \leq \phi(A(x,y))$, *where* $\phi \in \Psi$.

If T is k-continuous, then T possesses a fixed point z. Furthermore, T is continuous at z iff

$$\lim_{x \to z} A(x,z) = p(z,z).$$

3.1. Fixed- Disc Results

Definition 3.6. Let (X, p) be a partial metric space, and let $T : X \to X$ be a self-mapping. The set

$$C_{x_0,r} = \{x \in X : p(x, x_0) = r + p(x_0, x_0)\}$$

is referred to as a circle centered at x_0 with radius r. If every point x in $C_{x_0,r}$ satisfies $Tx = x$, then $C_{x_0,r}$ is known as fixed circle of the mapping T.

Definition 3.7. Let (X, p) be a partial metric space, and let $T : X \to X$ be a self-mapping. The set

$$D_{x_0,r} = \{x \in X : p(x, x_0) \leq r + p(x_0, x_0)\}$$

is termed a disk centered at x_0 with radius r. If $Tx = x$ holds for every $x \in D_{x_0,r}$, then $D_{x_0,r}$ is called a fixed disk under the mapping T.

Theorem 3.8. *Let (X, p) be a complete partial metric space, and let $T : X \to X$ be a self-mapping. Define the number r by*

$$r = \inf\{p(x, Tx) : x \notin F_T\}. \tag{6}$$

Suppose there exists a point $x_0 \in X$ such that for every $x \in X \setminus F_T$,

$$p(x, Tx) < A(x, x_0) \tag{7}$$

and

$$0 < p(x_0, Tx) \leq r + p(x_0, x_0), \tag{8}$$

Then the following conclusions hold:

(i) x_0 is a fixed point of T.

(ii) The mapping T fixes the disc $D_{x_0,r}$.

(iii) The mapping T fixes the circle $C_{x_0,r}$.

Proof. (i) Let $x_0 \in X \setminus F_T$. Afterward,

$$\begin{aligned}
p(x_0,Tx_0) < A(x_0,x_0) =& [p(x_0,x_0)]^{\beta}[p(x_0,Tx_0)]^{\alpha}[p(x_0,Tx_0)]^{\gamma}\left(\frac{p(x_0,Tx_0)+p(x_0,Tx_0)}{2}\right)^{1-\alpha-\beta-\gamma}\\
=& [p(x_0,x_0)]^{\beta}[p(x_0,Tx_0)]^{\alpha}[p(x_0,Tx_0)]^{\gamma}[p(x_0,Tx_0)]^{1-\alpha-\beta-\gamma}\\
=& [p(x_0,x_0)]^{\beta}[p(x_0,Tx_0)]^{1-\beta}\\
\implies [p(x_0,Tx_0)]^{\beta} <& [p(x_0,x_0)]^{\beta}\\
\implies p(x_0,Tx_0) <& p(x_0,x_0)
\end{aligned}$$

which contradicts (P2). Hence $x_0 \in F_T$.

(ii) Suppose $x \in D_{x_0,r}$ and $x \in X \setminus F_T$. Then

$$p(x,x_0) \leq r + p(x_0,x_0).$$

Using part (i), we have

$$\begin{aligned}
p(x,Tx) < A(x,x_0) =& [p(x,x_0)]^{\beta}[p(x,Tx)]^{\alpha}[p(x_0,Tx_0)]^{\gamma}\left(\frac{p(x,Tx_0)+p(x_0,Tx)}{2}\right)^{1-\alpha-\beta-\gamma}\\
=& [p(x,x_0)]^{\beta}[p(x,Tx)]^{\alpha}[p(x_0,x_0)]^{\gamma}\left(\frac{p(x,x_0)+p(x_0,Tx)}{2}\right)^{1-\alpha-\beta-\gamma}\\
\leq& [r+p(x_0,x_0)]^{\beta}[p(x,Tx)]^{\alpha}[r+p(x_0,x_0)]^{\gamma}[r+p(x_0,x_0)]^{1-\alpha-\beta-\gamma}\\
=& [r+p(x_0,x_0)]^{1-\alpha}[p(x,Tx)]^{\alpha}\\
\leq& [p(x,Tx)]
\end{aligned}$$

which is contradiction. So $x = Tx$. Hence T fixes the disc.
(iii) Similar to (ii). □

Theorem 3.9. *Let (X,p) be a complete partial metric space, and let $T : X \to X$ be a self-mapping. Define the number r by*

$$r = \inf\{p(x,Tx) : x \notin F_T\}, \tag{9}$$

where F_T denotes the set of fixed points of T. Assume that there exists a point $x_0 \in X$ such that, for every $x \in X \setminus F_T$, the following conditions are met:

$$p(x,Tx) < \phi(A(x,x_0)), \tag{10}$$

$$0 < p(x_0,Tx) \leq r + p(x_0,x_0). \tag{11}$$

Under these conditions, the following conclusions can be drawn:

(i) x_0 is a fixed point of the mapping T;

(ii) The disc $D_{x_0,r}$ is invariant under T;

(iii) The circle $C_{x_0,r}$ is also invariant under T.

Proof. Similar technique of Theorem 3.8. □

4. Conclusions

In conclusion, this work offers a new perspective on Rhoade's discontinuity problem by introducing a self-mapping with a fixed point that is discontinuous at the fixed point within a partial metric space. We have derived a few geometric properties of F_T under interpolative-type contraction, along with key findings related to fixed-disc and fixed-circle results. These contributions enhance our understanding of fixed point theory in spaces where discontinuities are present.

Acknowledgment

I would like to express my sincere gratitude to the reviewers for their valuable feedback and insightful comments, which greatly improved the quality of this manuscript. Their constructive suggestions and attention to detail were instrumental in enhancing my work.

References

[1] Asadi, M. **(2017)**. Discontinuity of control function in the (F, ϕ, θ)-contraction in metric spaces. *Filomat*, **31(17)**: 5427-5433.

[2] Aydi, H., Karapinar, E., & Roldan Lopez de Hierro, A. F. **(2019)**. w-Interpolative Cirić-Reich-Rus-Type Contractions. *Mathematics*, **7:** 57.

[3] Aydi, H., Chen, C. M., & Karapinar, E. **(2019)**. Interpolative Cirić-Reich-Rus type contractions via the Branciari distance. *Mathematics*, **7(1):** 1–7.

[4] Banach, S. **(1922)**. Sur les opérations dans les ensembles abstraits et leur application aux équations intégrales. *Fundamenta Mathematicae*, **3:** 133–181.

[5] Bisht, R. K., & Pant, R. P. **(2017)**. Contractive definitions and discontinuity at fixed point. *Appl. Gen. Topol.*, **18:** 173–182.

[6] Gaba, Y. U., & Karapinar, E. **(2019)**. A new approach to the interpolative contractions. *Axioms*, **8(4):** 1–4.

[7] Gautam, P., Mishra, V. N., Ali, R., & Verma, S. **(2020)**. Interpolative Chatterjea and cyclic Chatterjea contraction on quasi-partial b-metric space. *AIMS Mathematics*, **6(2):** 1727–1742.

[8] Kannan, R. **(1968)**. Some results on fixed points. *Bull. Calcutta Math. Soc.*, **62:** 71–76.

[9] Karapinar, E. **(2018)**. Revisiting the Kannan type contractions via interpolation. *Adv. Theory Nonlinear Anal. Appl.*, **2:** 85–87.

[10] Karapinar, E. **(2021)**. Interpolative Kannan-Meir-Keeler type contraction. *Advances in the Theory of Nonlinear Analysis and its Application*, **5(4):** 611–614.

[11] Karapınar, E., Alqahtani, O., & Aydi, H. **(2019)**. On interpolative Hardy-Rogers type contractions. *Symmetry,* **11(1):** 1–8.

[12] Matthews, S. G. **(1994)**. Partial metric topology. *Ann. New York Acad. Sci.*, **728:** 183–197.

[13] Meir, A., & Keele, E. **(1969)**. A theorem on contraction mappings. *J. Math. Anal. Appl.*, **28:** 326–329.

[14] Nazam, M., Aydi, H., & Hussain, A. **(2021)**. Generalized interpolative contractions and an application. *Journal of Mathematics*, **2:** 1–13 .

[15] Pant, A., & Pant, R. P. **(2017)**. Fixed points and continuity of contractive maps. *Filomat,* **31(11):** 3501–3506.

[16] Pant, R. P. **(1999)**. Discontinuity and fixed points. *J. Math. Anal. Appl.,* **240:** 284–289.

[17] Rhoades, B. E. **(1988)**. Contractive definitions and continuity. *Contemp. Math.,* **72:** 233–245.

[18] Rhoades, B. E. **(1977)**. A comparison of various definitions of contractive mappings. *Trans. Am. Math. Soc.,* **226:** 257–290.

[19] Tas, N. **(2023)**. Interpolative contractions and discontinuity at fixed point. *Appl. Gen. Topol.,* **24(1):** 145–156.

Instruction to Authors
Nepal Journal of Mathematical Sciences (NJMS)

1. Scope

Nepal Journal of Mathematical Sciences (NJMS) is the official peer-reviewed journal published by the School of Mathematical Sciences, Tribhuvan University. It is devoted to publishing original research papers as well as critical survey articles related to all branches of pure and applied mathematical sciences. The journal aims to reflect the latest developments in issues related to Applied Mathematics, Mathematical Modelling, Industrial Mathematics, Biomathematics, Pure and Applied Statistics, Applied Probability, Operations Research, Theoretical Computer Science, Information Technology, Data Science, Financial Mathematics, Actuarial Science, Mathematical Economics and many more disciplines. NJMS is published in English and it is open to authors around the world regardless of nationality. It is published two times a year. NJMS articles are freely available online and in print form.

2. Editorial Policy

NJMS welcomes high-quality original research papers and survey articles in all areas of Mathematical Sciences and real-life applications at all levels including new theories, techniques and applications to science, industry, and society. The authors should justify that the theoretical as well as computational results they claim really contribute to Mathematical Sciences or in real- life applications. A complete manuscript be no less than 5 pages and no more than 20 pages (11pt, including figures, tables, and references) as mentioned in the paper Template. However, this can be extended with the acceptance of the respective referees and the Editor-in-Chief. The submitted manuscript should meet the standard of the NJMS.

3. Manuscript Preparation

Manuscript must be prepared in Microsoft Word format (see Template) and LATEX (see template) in the prescribed format with a given page limit.

4. Title of the Paper

The title of the paper should be concise, and specific, not exceeding 15 words in length.

5. Authors Names and Institutional Affiliations

This should include the full names, institutional addresses, and email addresses of authors. The corresponding author should also be indicated.

6. Abstract and Keywords

Each article is to be preceded by an abstract up to a maximum of 250 words with 4-6 key pertinent words.

7. Introduction

The introduction briefly describes the problem, purpose, significance, and output of the research work, including the hypotheses being tested. The current state of the research field should be reviewed carefully and key publications should be cited.

8. Materials and Methods

It describes the research plan, the materials (or subjects), and the method used. It explains in detail the data, sample and population, and the variables used.

9. Results and Discussions

The results section should provide details of all of the experiments that are required to support the conclusions. Discussion can also be combined with results.

10. Figures and Tables

Figures and Tables are to be separately numbered, and titled in the text serially.

11. Conclusions and Acknowledgments

Not mandatory, but can be added to the manuscript.

12. References

•Journal Citation

[1] Faraji, H. & Nourouzi, K. (2017). Fixed and common fixed points for (ψ, ϕ)-weakly contractive mappings in b-metric spaces. *Sahand Communications in Mathematical Analysis*.**7(1):** 49-62.

•Doctoral Dissertation Citation

[1] Oliver, T. H. (2009). *The Ecology and Evolution of Ant-Aphid Interactions* (Doctoral dissertation Imperial College London).

•Research Book Citation

[1] Mursaleen, M. and Başar, F. (2020). *Topics in Modern Summability Theory*. BocaRaton : CRC Press.

13. Manuscript Submission

At the time of submission, authors are requested to include a list of 3-5 panelists of experts in the related research area. All information, submissions, and correspondence of the articles should be addressed to

Mailing Address: njmseditor@gmail.com

Nepal Journal of Mathematical Sciences (NJMS)

ISSN: 2738-9928 (Online), 2738-9812 (Print)

Volume 6, Number 1, February 2025

CONTENTS

Mailing Address:

Nepal Journal of Mathematical Sciences
School of Mathematical Sciences
Tribhuvan University, Kirtipur, Kathmandu, Nepal

Phone: (00977) 01-6200207

Website: www.sms.tu.edu.np

Email: *njmseditor@gmail.com*

The Nepal Journal of Mathematical Sciences (NJMS) is now available on NepJOL at https://www.nepjol.info/index.php/njmathsci/index